Supercharging Accelerates T-Tubule Membrane Potential Changes in Voltage Clamped Frog Skeletal Muscle Fibers

Albert M. Kim and Julio L. Vergara

Department of Physiology, University of California at Los Angeles, Los Angeles, California 90095-1751 USA

ABSTRACT   In voltage-clamp studies of single frog skeletal muscle fibers stained with the potentiometric indicator 1-(3-sulfonatopropyl)-4-[β[2-(di-n-octylamino)-6-naphthyl]vinyl]pyridinium betaine (di-8 ANEPPS), fluorescence transients were recorded in response to both supercharging and step command pulses. Several illumination paradigms were utilized to study global and localized regions of the transverse tubule system (T-system). The rising phases of transients obtained from global illumination regions showed distinct accelerations when supercharging pulses were applied (95% of steady-state fluorescence achieved in 1.5 ms with supercharging pulses versus 14.6 ms with step pulses). When local transients were recorded at the edge of the muscle fiber, their kinetics resembled those of the applied waveform, but a similar relationship was not observed in transients from regions near the edge chosen to minimize the surface membrane contribution. We developed a model of the T-system capable of simulating membrane potential changes as a function of time and distance along the T-system cable and the associated fluorescence changes in regions corresponding to the experimental illumination strategies. A critical parameter was the access resistance term, for which values of 110–150 $\Omega \cdot cm^2$ were adequate to fit the data. The results suggest that the primary mechanism through which supercharging pulses boost the kinetics of T-system voltage changes most likely involves their compensating the voltage attenuation across the access resistance at the mouth of the T-tubule.

INTRODUCTION

The central role of the transverse tubular system (T-system) in skeletal muscle excitation-contraction (E-C) coupling has been recognized since Huxley and Taylor's early "local activation" experiments (Huxley and Taylor, 1958). Their conclusion, that contraction followed T-system depolarization rather than surface membrane depolarization, has since been confirmed and expanded by numerous studies reporting on the nature of the T-system. In particular, several results implicate its behavior as an active network with a sodium conductance contributing to action potential propagation radially into the muscle fiber (Adrian et al., 1969a,b; Gonzalez-Serratos, 1971; Bezanilla et al., 1972; Bastian and Nakajima, 1974). Membrane depolarization during the T-system action potential initiates a signaling pathway that results in Ca^{2+} release from the sarcoplasmic reticulum (SR) within a few milliseconds (Palade and Vergara, 1982; Vergara and Delay, 1986).

To study the voltage dependence of this dynamic process, investigators have typically voltage-clamped individual fibers whose T-systems are rendered passive by blocking the relevant conductances (e.g., Na^+ and K^+). As a passive network, the T-system can be represented electrically as a large distributed capacitance isolated from the surface membrane by an access resistance (Adrian and Peachey, 1973; Heiny et al., 1983) and a distributed T-tubule lumen resis-

tivity (Falk and Fatt, 1964; Adrian et al., 1969a; Ashcroft et al., 1985). However, these features impart an experimental limitation to the electrophysiological characterization of tubular membranes: voltage changes in the T-system may differ significantly in speed and amplitude from the command potential imposed at the surface. For example, in response to the traditional step change in potential applied at the surface, the average T-system potential reaches a steady-state value only after 20–30 ms (Vergara and Bezanilla, 1981; Heiny and Vergara, 1982; Ashcroft et al., 1985; Jong et al., 1997). This time-variant input to the E-C coupling machinery makes step command-elicited responses—e.g., charge movements or Ca^{2+} transients—difficult to interpret on the time scale of an action potential.

Following previous studies using potentiometric dyes in skeletal muscle (Vergara et al., 1978; Nakajima and Gilai, 1980; Vergara and Bezanilla, 1981; Heiny and Vergara, 1982, 1984; Heiny et al., 1983; Vergara and Kim, 1997), we recently reported that supercharging command pulses (Armstrong and Chow, 1987) can be used to rapidly (<2 ms) establish voltage steps in the T-system (Vergara and Kim, 1997). As a result, the Ca^{2+} transients and charge movement currents recorded are significantly accelerated (Kim and Vergara, 1998). The current work further contrasts how supercharging and step command pulses effect voltage changes on surface and T-system membranes. We chose the fluorescent potentiometric dye 1-(3-sulfonatopropyl)-4-[β[2-(di-n-octylamino)-6-naphthyl]vinyl]pyridinium betaine (di-8 ANEPPS) as an optical probe of the T-system and surface membrane of muscle fiber segments because of its stable staining of extracellular membranes, low toxicity, and large changes in fluorescence (Bedlack et al., 1992; Rohr and Salzberg, 1994).

Applying the supercharging and step voltage pulse paradigms to muscle fibers stained with di-8 ANEPPS elicited fluorescence transients whose kinetics and amplitudes were compared. The boosted rates of change achieved with supercharging pulses were further characterized by fluorescence detected from several localized illumination regions chosen to address the contribution of the surface membrane fluorescence and the influence of the T-system's cable properties. The results were interpreted using a radial cable model of the T-system that incorporated algorithms accounting for illumination intensities in a thick preparation. Our analysis provides an experimental and theoretical examination of the supercharging methodology and demonstrates that depolarization of the passive T-system can be established quickly, on the same time scale as action potential-induced E-C coupling (<5 ms).

Portions of this work have appeared previously in abstract form (Vergara and Kim, 1997).

MATERIALS AND METHODS

Solutions

All experiments were carried out with the following solutions. Isotonic K_2SO_4 solution: 80 mM K_2SO_4, 10 mM potassium 3-(N-morpholino)propanesulfonic acid (K-MOPS); titrated to pH 7.0 with KOH, osmolality = 238 mmol/kg. Internal solution: 90 mM Cs-aspartate, 20 mM tetraethylammonium hydroxide (TEA-OH), 20 mM Cs-MOPS, 5 mM Na_2-phosphocreatine, 5 mM ATP-Na_2, 1 mM $MgSO_4$, 0.1 mg/ml creatine phosphokinase, 5–20 mM EGTA; titrated to pH 7.0 with CsOH, osmolality = 264 mmol/kg. External solution: 160 mM TEA-OH, 10 mM MOPS, 5 mM Cs-MOPS, 3.25 mM Ca-SO_4, 2 mM $CdCl_2$, 0.5 μM tetrodotoxin; titrated to pH 7.0 with H_2SO_4, osmolality = 260 mmol/kg. The conductivity of the external solution was measured to be 0.01 S·cm^{-1} at 15°C with a conductivity cell and bridge (models 3401/31, respectively; Yellow Springs Instruments, Yellow Springs, OH).

General procedure

The experiments were performed using cut single muscle fibers isolated from the semitendinosus muscle (dorsal head) of *Rana catesbeiana*. The frogs were killed by rapid transection of the cervical spinal cord, followed quickly by pithing first in the cranial and then caudal direction. Fiber preparation and mounting protocols are similar to those reported previously (Hille and Campbell, 1976; Vergara et al., 1978; Heiny and Vergara, 1982; Palade and Vergara, 1982). Briefly, single fiber segments $\sim$1.5–3 cm in length and 70–170 μm in diameter were dissected, preserving the tendon insertions on one end. The individual segments were extracellularly stimulated, and only those able to respond with all-or-nothing fast twitches were selected. These segments were isolated, mounted, and stretched slightly in a small plastic dish lined with Sylgard (Dow Corning 182; Dow Corning, Midland, MI). The Ringer's solution used for dissection was then exchanged for the isotonic K_2SO_4 solution, inducing the fiber segments to undergo a K contracture, after which they spontaneously relaxed. The relaxed segments were mounted on a triple Vaseline gap chamber as described previously (Vergara et al., 1978), and the solutions in the cut end pools were replaced by the internal solution listed above. Small pieces of transparent plastic film were placed over the fiber in the experimental pools. This ensured constant fluid levels in each pool and a homogeneous liquid-film interface without potential air-liquid optical aberrations in the electrical/optical measuring pool. The cut ends were permeabilized by exposure to an internal solution containing 80 μg/ml saponin for 1–2 min, followed by washing with normal internal solution. Fibers were then repolarized by exchanging the measuring pool solution with the external solution described above.

Fiber staining

For potentiometric studies, fibers were stained for 1–2 h with 0.1–5 μM di-8 ANEPPS (Molecular Probes, OR) dissolved in isotonic K_2SO_4 solution before they were mounted on the chamber. This combination of staining time and dye concentration was found to give optimal signal with low toxicity (as assessed by nonlinear leak currents smaller than 40 nA). The dye solution was prepared fresh before every experiment by initially dissolving a few crystals of di-8 ANEPPS in 2–4 μl of 25% Pluronic 127 (Molecular Probes) in dimethyl sulfoxide. The solvent-crystal mixture was briefly heated to increase the dye's solubility. This small volume of dissolved dye was then mixed into warm ($\sim$30–35°C) isotonic K^+ solution to achieve the final concentration. The actual values for dye concentrations were determined by measuring the absorption peaks of the staining solutions in a spectrophotometer (model 8453; Hewlett-Packard, Van Nuys, CA) and calculating the molar concentration, using the published extinction coefficient of di-8 ANEPPS (35×10^3 cm^{-1}M^{-1}; Molecular Probes). All experiments were performed at 15°C.

The confocal image in Fig. 1 *A* shows the typical fluorescence pattern seen after a single muscle fiber is stained by the above protocol. It displays bright fluorescence at the edges of the fiber associated with the sarcolemma, and a banded appearance reflecting relatively homogeneous staining of the T-system. This demonstrates that, away from the fiber borders, the T-system is the primary source of fluorescence. The sarcomere length is $\sim$5 μm.

Optical signal detection

The triple Vaseline gap chamber was mounted on the stage of an upright microscope as described (Heiny and Vergara, 1982). In a configuration similar to that described previously (Vergara et al., 1991), epifluorescence illumination was provided by a 150-W tungsten lamp and focused onto the preparation with a 20$\times$ objective (Fluo20, NA 0.75; Nikon, Tokyo, Japan). Objectives with higher numerical apertures and magnifying powers could not be used with the current electrophysiological/optical system because of limitations imposed by their small working distances. Brief (<1 s) periods of illumination were synchronized with the electrophysiological pulses by using an electronic shutter (Uniblitz VS25S1S1; Vincent Associates, Great Neck, NY) under software control. We used several strategies of illumination, as illustrated in Fig. 1 *B*. These were: Global—a roughly ellipsoid region of the fiber with a width of $\sim$100 μm; Center—a circular region $\sim$30 μm in diameter located in the middle of the fiber; Edge-tangent—a circular region $\sim$30 μm in diameter whose perimeter was tangential to the fiber border, so that the contribution of surface membrane fluorescence was minimized; Edge—a semicircular region at the edge of the fiber with a short diameter of $\sim$15 μm and a long diameter of $\sim$30 μm. Regions were created by adjusting the diaphragm in the epifluorescence light path and by moving the location of the muscle fiber with respect to the illuminating beam. When measurements were made between nonglobal regions in the same fiber, resting fluorescence levels were matched so that comparisons were made between volumes of similar illumination intensity.

Fluorescence was measured using a 480DF60 excitation filter (Omega Optical, Brattleboro, VT), a 560DCLPO2 dichroic mirror (Omega Optical), and a 590LP or 610LP emission filter. Fluorescence emission was detected with a PIN photodiode (HR-020; UDT, Hawthorne, CA) whose output signal was connected to the headstage of a standard patch-clamp amplifier (Axopatch 1B, 100-GΩ feedback resistor; Axon Instruments, Foster City, CA). The electronic noise of the detector-amplifier system was typically 0.18 pA RMS referred to the input at 2-kHz bandwidth. Analog fluorescence signals were filtered preacquisition at 2 kHz with an 8-pole Bessel filter (model 902; Frequency Devices, Haverhill, MA) and postacquisition with a 2-kHz digital low-pass FFT filter (Origin 5.0; Microcal Software,
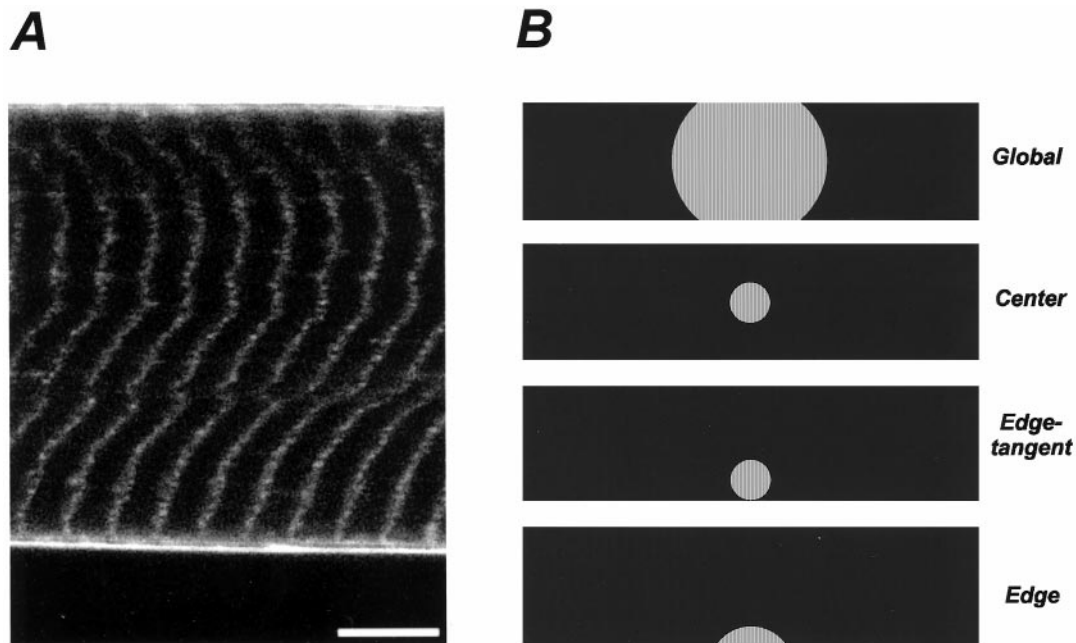
A

B

FIGURE 1　T-system staining pattern and illumination regions. (*A*) Confocal scanning image of a skeletal muscle fiber stained with di-8 ANEPPS. Scale bar is 10 μm. The image was acquired with a Bio-Rad MRC600 scanning confocal microscopy system using a 100× objective (1.3 NA; Nikon, Japan). The raw image was stretched to optimal range with the Intellihance GS algorithm in Corel PhotoPaint 7 (Corel Corporation, Ottawa, Canada). (*B*) Schematic of illumination paradigms used during experiments. Fiber diameter $\approx$ 100 μm. Not drawn precisely to scale.

Northampton, MA). Membrane depolarizations resulted in fluorescence increases (ΔF), plotted throughout the paper as upward deflections.

Voltage-clamp protocol and data acquisition

Voltage clamping was performed as described previously (Hille and Campbell, 1976; Vergara et al., 1978; Heiny and Vergara, 1982; Palade and Vergara, 1982). Command pulses were applied and data were acquired via a multifunction PC AT board with 16-bit D/A and A/D converters (AT-MIO16 XE-10; National Instruments, Austin, TX), using custom software (AKLAMP 1.4; Kim and Vergara, unpublished) written in the LabVIEW G environment (LabVIEW 4.01; National Instruments). In most cases, voltage, current, and fluorescence signals were acquired simultaneously. Unless otherwise indicated, analog signals were filtered before acquisition

with an 8-pole Bessel filter (model 902; Frequency Devices) set at less than one-half of the sampling frequency (20–50 kHz).

Supercharging command pulses (Fig. 2) consisted of a step voltage pulse summed with a triexponential decay waveform. We adjusted (tuned) values for time constants (τ_1-τ_3) and amplitudes (A_1-A_3) of the exponential components such that a quasistep of voltage was detected in the T-system. Throughout this paper, the functional definition of a quasistep is that the evoked potentiometric fluorescence transient achieved 95% of the steady-state value in <2 ms (see Results).

Data analysis and statistics

Data were analyzed and graphed using Origin 5.0 (Microcal Software), Excel97 (Microsoft Corporation, Redmond, WA), or custom routines writ-

FIGURE 2　Relationship between the conventional step voltage-clamp waveform and a typical supercharging waveform. The conventional step pulse waveform and a digitally created boosting waveform typical of our experiments are shown. The time constants for each of the three unique exponential decays in the boosting waveform are as noted, and their weightings are given as a percentage value of the applied step voltage change. In this case, a 100-mV step pulse is summed with a boosting waveform with time constants of 1.0 (100%), 3.2 (50%), and 40 (5%) ms. The resulting waveform is defined as a 100-mV supercharging pulse.

100 mV Step Pulse　　　Boosting waveform
Σ of 3 exponential decays　　　100 mV Supercharging Pulse

100 mV

25 ms

+

=
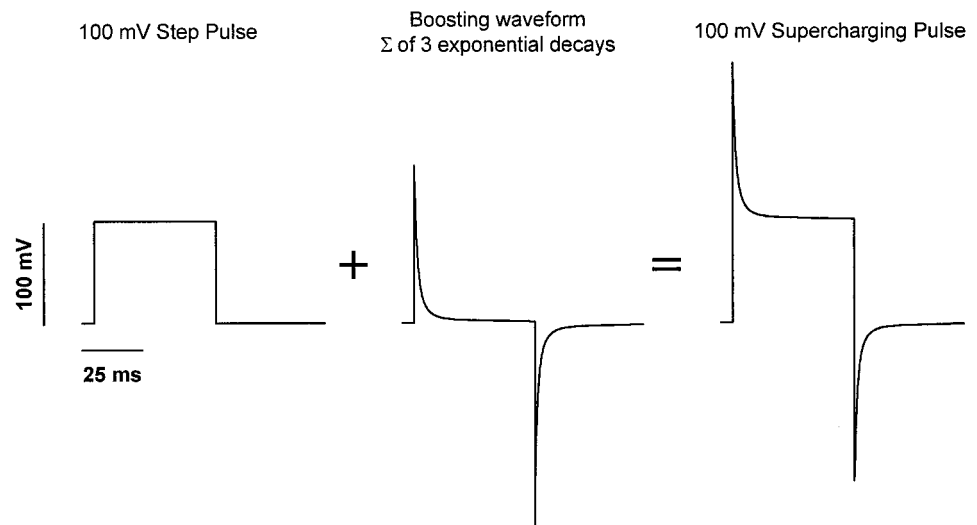
ten in G (LabVIEW 4.0.1; National Instruments). Unless otherwise stated, average values are given $\pm$ the standard deviation.

Modeling

T-system optical signals were interpreted with the aid of a distributed cable equivalent circuit model (Adrian et al., 1969a; Adrian and Peachey, 1973; Ashcroft et al., 1985) that described the passive electrical properties of the T-system as a radially symmetrical network. The model was implemented in Fortran 77 and in G, and integrated numerically by an implicit Crank-Nicolson method (Crank and Nicolson, 1947; Crank, 1975; Gerald, 1978). For complete details of the mathematics and computer algorithms, see Appendices A and B.

RESULTS

Kinetic and steady-state analysis

When step and supercharging voltage clamp pulses were applied to stained fibers, the elicited fluorescence transients demonstrated distinct kinetic differences. Fig. 3 *A* displays a family of global illumination transients (*lower traces*) recorded in response to a series of 50-ms step waveforms (*upper traces*). The fluorescence traces show a fast early jump in the first millisecond after pulse application, followed by a slower rise during the remainder of the pulse. When fit with a single exponential function (see *continuous trace* in Fig. 3 *C*), the average time constant (τ) for these traces is 5.4 ± 0.4 ms ($n = 5$ traces). This assumed function predicts that step pulses reach ~95% of steady-state fluorescence in 16.2 ± 1.2 ms (3τ). A similar value was obtained from a larger population of step-induced transients (14.6 ± 1.8 ms, $n = 11$ from four different fibers). In contrast, Fig. 3 *B* illustrates that the recorded fluorescence reaches a steady state much more quickly in response to tuned supercharging pulses. The transients show a quasistep time course, with the evoked fluorescence rapidly rising with a $\tau = 0.5 \pm 0.03$ ms ($n = 5$ traces; cf. *dotted trace* in Fig. 3 *C*). It follows that the calculated time to achieve ~95% of steady-state fluorescence for these traces is 1.5 ± 0.09 ms. In 18 traces from five different fibers, the analogous calculated result for 95% of steady state was almost identical (1.5 ± 0.37 ms).

An expanded time scale view (Fig. 3 *C*) more clearly exhibits the accelerated potential change that supercharging affords when compared to step-induced change. The +10 mV fluorescence transients from Fig. 3, *A* and *B*, are superimposed to show the early events after pulse initiation. After the onset of the command pulse, the supercharging (*upper*) trace rises more quickly than its step counterpart (*lower trace*). Moreover, it reaches 95% of the steady value within 2 ms (quasistep behavior), whereas the step-elicited fluorescence continues to change over the entire interval plotted (12 ms). Hence, as reported by global transients, the average T-system depolarizations achieved by tuned supercharging pulses more closely resemble the theoretically ideal "step change" in potential than do those seen in response to step pulses.

To test the scalability of our pulse protocols and di-8 ANEPPS evoked fluorescence signals, we investigated the steady-state dye response to pulses of various amplitudes. Recorded fluorescence was averaged over the last 5 ms of a 50-ms step and supercharging pulses applied over a range of voltages in both depolarizing and hyperpolarizing directions. Fig. 4 shows a scatter plot of the results of this analysis in five fibers. It can be seen that the magnitude of fluorescence obtained in response to step and supercharging pulses was linear ($R = 0.99$) regardless of pulse polarity. Furthermore, the standard error is generally small (within the size of the symbols), even at the more extreme positive and negative test potentials, giving no evidence for voltage-dependent nonlinearities.

Tuning supercharging command pulse parameters

To converge on the optimally tuned waveforms shown in Fig. 3 *C*, it was necessary to specify quantitatively the supercharging parameters (τ_1-τ_3 and A_1-A_3; see Appendix A) for each fiber. As a first approximation, the capacitive phase of the current recorded in response to a 50-ms, 50-mV depolarizing step pulse was fit with a three-phase exponential decay function (data not shown). Based on control global detection experiments, choosing τ_1-τ_3 values to match the fitted time constants resulted in poor compensation, regardless of the amplitude parameters selected. The efficacy of each waveform in establishing a quasistep was more sensitive to changes in τ_2 than to those in τ_1 or τ_3 over the ranges of values tested. Varying τ_2 according to the fitted value of the middle time constant (typically in the range of 2–6 ms) and fixing τ_1 and τ_3 at ~1.0 ms and ~40.0 ms led to better consistency in attaining quasisteps. Typically 5–10 trials per experiment were necessary to achieve optimal tuning of pulse parameters.

The properties of correctly tuned waveforms are summarized in Table 1. Amplitudes of the supercharging components (A_1-A_3) showed larger variability than the τ's, with A_1 showing the largest, followed by A_2 and A_3 (Table 1). Adjusting τ_1 and A_1 was essential for accelerating the initial jump in T-system potential; τ_2 and A_2 were most pertinent to the transition from early spike to steady-state plateau; and τ_3 and A_3 correlated best with the small leak current associated with each fiber. Decreasing τ_1 below 1.0 ms had no perceptible influence on the performance of the command pulse, whereas increasing it proved less effective in obtaining a quasistep in T-system potential.

We also investigated how overcompensation might manifest itself by using incorrectly tuned waveforms. As illustrated in Fig. 5, poorly chosen command pulse parameters can indeed result in overcharging the T-system. The "Step" and correctly tuned "Super" pulses evoke fluorescence transients similar to those seen in Fig. 3, in that the former depolarizes the T-system with a small early rise followed by a slower increase in fluorescence, and the latter generates a
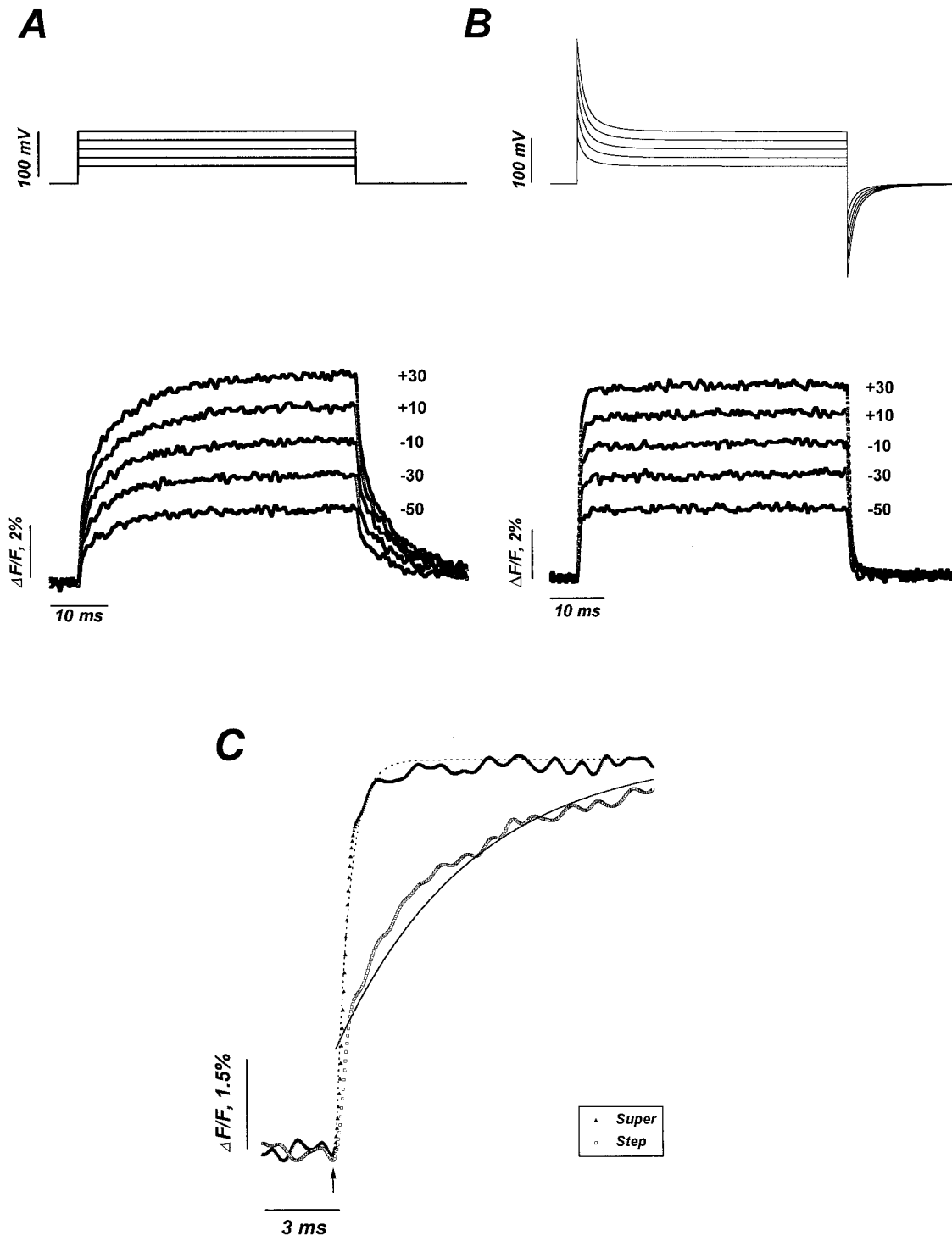
FIGURE 3 Waveforms and global illumination fluorescence transients for step and supercharging pulses. (*A, upper traces*) Family of five-step voltage waveforms applied from a holding potential of -90 mV. Pulse amplitudes ranged from 40 to 120 mV, in increments of 20 mV. (*Lower traces*) Corresponding fluorescence elicited by the family of voltage pulses. The absolute potential was achieved by voltage command pulses indicated for each transient. Each trace was signal averaged ($n = 5$). (*B, upper traces*) Family of five supercharging voltage waveforms applied from a holding potential of -90 mV. Pulses were digitally created as described in Materials and Methods (cf. Fig. 2), and their amplitudes ranged from 40 to 120 mV, in increments of 20 mV. (*Lower traces*) Corresponding fluorescence elicited by the family of voltage pulses. Traces are labeled and averaged as in *A*. Supercharging parameters: $\tau_1 = 1.0$ ms, 120%; $\tau_2 = 3.0$ ms, 60%; $\tau_3 = 40.0$ ms, 5%. (*C*) Superimposed step (□) and supercharging (▲) global transients shown on an expanded time scale. Continuous (step) and dotted (super) lines represent least-squares fits to the traces shown, using a function of the form

$$y(t) = y_0 + A(1 - e^{-t/\tau})$$

For the step case $y_0 = 1.8\%$, $A = 5.1\%$, and $\tau = 5.5$ ms; in the supercharging case $y_0 = 0.03\%$, $A = 6.8\%$, and $\tau = 0.54$ ms. The arrow indicates the start of the stimulus pulse. Fiber diameter $= 170$ μm.
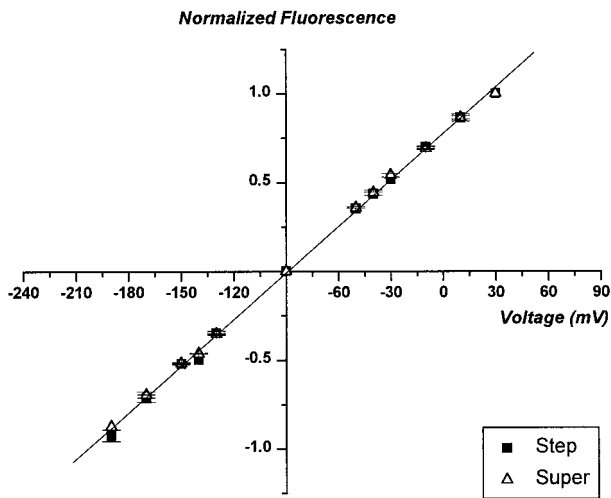
Normalized Fluorescence

FIGURE 4 Scatter plot of steady-state fluorescence. ■, Step pulse data. △, Supercharging data. $\Delta F/F$ values were normalized to the steady-state fluorescence seen in response to a 50-ms step or supercharging pulses to +30 mV in each particular fiber ($\Delta F/F_{+30}$). The step $\Delta F/F_{+30}$ and super $\Delta F/F_{+30}$ values were not statistically different ($p > 0.6$, two-tailed Student's t-test). Each data point is the average of two to five values, each of which in turn is the average of five traces obtained at the given test potential. Error bars represent ±SEM, $n = 2$–5, from five fibers. The straight line is a linear regression fit through the average of the step and super data sets constrained to intersect the y axis at the holding potential, −90 mV.

quasistep in T-system potential. However, the "Over" command pulse induces a large initial rise in fluorescence that decays to the steady-state plateau ($\tau = 5.9$ ms). The degree of overcompensation shown in the "Over" transient as compared to the "Super" requires that an enormous voltage be applied initially (255% versus 135% over the original 100-mV step pulse, respectively). Thus overcompensation of the average T-system voltage will not readily result unless there are large errors in the choice of parameters.

Evoked fluorescence from different illumination regions

It might be argued that the global fluorescence quasisteps achieved by tuned supercharging waveforms could actually reflect membrane voltage contributions from grossly overcharged surface membrane and peripheral T-system regions that kinetically counterbalance undercompensated inner T-system regions. To explore this possibility, we devised a procedure to obtain localized fluorescence transients (see Materials and Methods, Fig. 1 B). Fig. 6 shows four sets of superimposed transients obtained using Global, Edge, Edge-tangent, and Center illumination while the fiber was stimulated with 120-mV step and supercharging command pulses. Traces from the Global region are similar to the records shown in Fig. 3, A and B, demonstrating the characteristic acceleration in depolarization kinetics achieved through a supercharging command pulse versus a conventional step pulse. The former induces a quasistep in average

T-system (plus surface membrane) potential, but the latter charges the T-system more slowly, with the evoked fluorescence creeping to steady state in >20 ms.

Transients from the Edge region differ from their Global counterparts considerably (Fig. 6 A). The Edge region supercharging transient shows an early spike in fluorescence that initially overshoots and then decays to the steady-state level in ~10 ms, and the Edge step transient rises quickly to the steady-state value within ~2 ms, but without an overshoot. Given the geometry of the illumination region, it is expected that the kinetic features of these traces reflect a weighted combination of surface and peripheral T-system contributions. But are these signals kinetically distinct from one another?

The Edge-tangent illumination scheme addresses this question by increasing the proportion of the T-tubular membrane contributing to the overall signal (cf. Fig. 1 A). Remarkably, transients from this region exhibit characteristics more akin to those obtained using Global as opposed to Edge illumination. The fluorescence trace elicited by the step pulse follows a time course showing a slow rise to steady state, as seen in the Global panel, rather than the more rapid rise seen in the Edge step case. Similarly, the supercharging record from the Edge-tangent region shows little evidence of the overshoot seen in the Edge trace. Rather, it illustrates a quasistep in fluorescence whose rising phase appears slightly rounded when compared to the Global transient. It is important to note that Edge-tangent transients rise with a time course ($\tau = 0.7 \pm 0.3$ ms, $n = 3$ different fibers) comparable to Global transients ($\tau = 0.5 \pm 0.12$ ms, $n = 5$ different fibers) in response to supercharging pulses. Furthermore, despite the fact that the Edge and Edge-tangent illumination regions overlapped by 30–50% (but with the latter avoiding the edge surface membrane), transients from these regions showed strikingly different kinetics.

A surprising finding was that Center region transients showed kinetics only marginally different from those obtained from the nonoverlapping Edge-tangent region (Fig. 6 A). This may imply that the voltage gradients along the T-system cable are minimal, or that Center illumination transients may not appropriately report the electrical behavior of inner T-tubule regions. In either case, the superimposed traces in Fig. 6 A demonstrate that, when compared with step pulse depolarization, supercharging pulses induce an acceleration that is evident in every illumination scheme.

Model predictions for different regional transients

To interpret the ramifications of the experimental data, it was necessary to develop a quantitative model that could predict not only the electrical behavior of the T-system in response to voltage clamp pulses, but also the potentiometric fluorescence emitted from illumination regions such as those outlined in Fig. 1 B. To address voltage changes in the T-system, we based our model on a version of the distrib-

TABLE 1 Summary of fiber characteristics and quasistep tuned supercharging parameters

	Fiber diameter (μm)	Sarcomere length (μm)	Capacitance (μF/cm^2)	τ_1 (ms)	τ_2 (ms)	τ_3 (ms)	A_1 (%)	A_2 (%)	A_3 (%)
Average ($n = 17$)	129	3.9	12.8	1.0	3.4	41.0	87.0	51.5	4.7
SD ($n = 17$)	27	0.2	2.4	0	0.8	2.3	30.0	13.7	1.0
Range	73–170	3.6–4.0	7.2–16.4	1.0	2.7–6.2	40–50	30–120	20–70	2–5

uted radial cable model (Adrian et al., 1969a) that was extended to include an access resistance (Adrian and Peachey, 1973; Ashcroft et al., 1985) and allow for supercharging voltage pulse inputs (see Appendix A). In addition, we incorporated algorithms that could account for varying illumination intensities through the fiber volume and different illumination paradigms (see Appendix B).

Traces from simulations using the model with parameters that matched the experimental conditions used in Fig. 6 *A* are plotted in Fig. 6 *B*. With the exception of the Center region, it can be seen that the model predictions agree quantitatively with the experimental records of Fig. 6 *A* in every illumination region. Each pair of traces shows the distinct acceleration of supercharging pulses (*continuous*
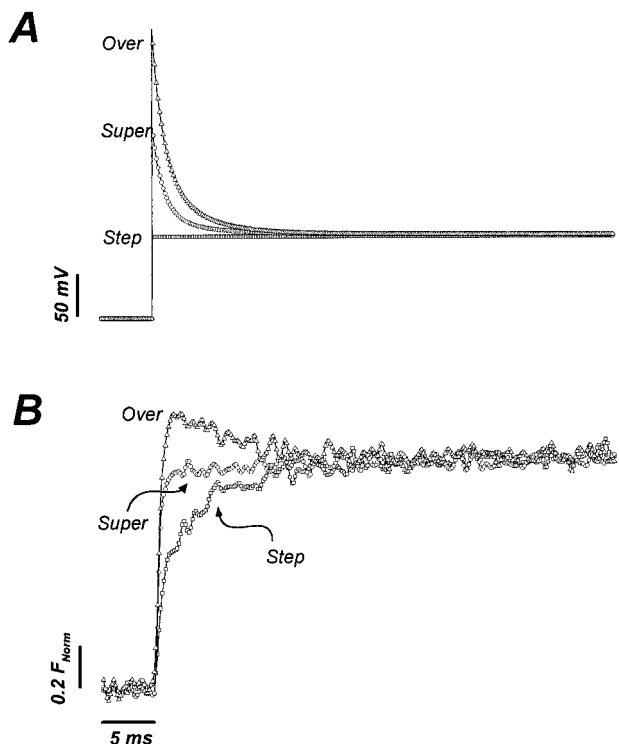

FIGURE 5 T-system global fluorescence response to different voltage command waveforms. (*A*) Three digitally created voltage clamp pulses are shown: a 100-mV step command waveform (□), a tuned 100-mV supercharging waveform (○) ($\tau_1 = 1.0$ ms, 100%; $\tau_2 = 3.2$ ms, 30%; $\tau_3 = 40.0$ ms, 5%), and an overcompensated 100-mV supercharging waveform (△) ($\tau_1 = 1.0$ ms, 150%; $\tau_2 = 3.2$ ms, 100%; $\tau_3 = 40.0$ ms, 5%). (*B*) Fluorescence transients recorded in response to waveforms in *A*. Symbols correspond to waveforms as in *A*. Traces are signal averaged ($n = 5$) and are shown normalized to the steady-state fluorescence as calculated by averaging the recorded values over the last 5 ms of a 50-ms pulse. Fiber diameter = 138 μm.

traces) over step pulses (*dotted traces*). For both types of pulses, Center simulations display slower rising phases than the corresponding experimental data.

Fig. 7 allows a direct comparison between the transients recorded from localized regions and the analogous model predictions. When superimposed, the data traces in Figs. 7 *A* again illustrate the striking difference in the fluorescence signal as seen in the Edge region compared with the Edge-tangent and Center regions. By drastically reducing the contribution of illuminated surface membrane, the properties of the detected signals are altered such that evidence of the supercharging overshoot applied at the surface is no longer apparent. This phenomenon is reproduced well in the Edge and Edge-tangent model simulations shown in Fig. 7 *C*. There are two model features necessary to predict the disparity between these traces. First, there must be a significant electrical isolation between surface membrane and the edge region of the T-system. This was attained by using access resistance (R_s) values in the range of 110–150 $\Omega \cdot$ cm^2 (145 $\Omega \cdot$ cm^2 in Figs. 6 and 7). Second, an appropriate estimate of the surface membrane contribution to the overall regional fluorescence is required. In the Edge region this was found to be 60%, whereas in the Edge-tangent region only 10% was used. Using the identical values for R_s and surface membrane contribution in each regional comparison, data and model predictions in response to step pulses (Fig. 7, *B* and *D*, respectively) are in similar quantitative agreement.

Curiously, the kinetic differences between the Edge-tangent and Center region model predictions (Fig. 7, *C* and *D*) are more marked than those apparent in the recorded fluorescence (Fig. 7, *A* and *B*). The Center illumination model predictions suggest that potentiometric fluorescence transients from more central T-system regions should follow a significantly slower time course than more peripheral regions, but this was not obvious from the data. In an attempt to reduce radial voltage gradients along the T-system, we ran simulations (data not shown) with T-tubule luminal conductivity (G_L) values up to fivefold greater than that of the external solution. Under these conditions, we were able to obtain a high degree of homogeneity between Edge-tangent and Center regions, but the resulting Edge-tangent traces showed slower kinetics than the data in Figs. 6 *A* and 7 *A*.

Matching model predictions with Edge-tangent transients in response to supercharging pulses provides specific evidence for a significant R_s. As shown in Fig. 8 *A* (same data as Figs. 6 *A* and 7), evoked fluorescence rises rapidly ($\tau = 0.7$ ms) and without an initial overshoot. Transients from
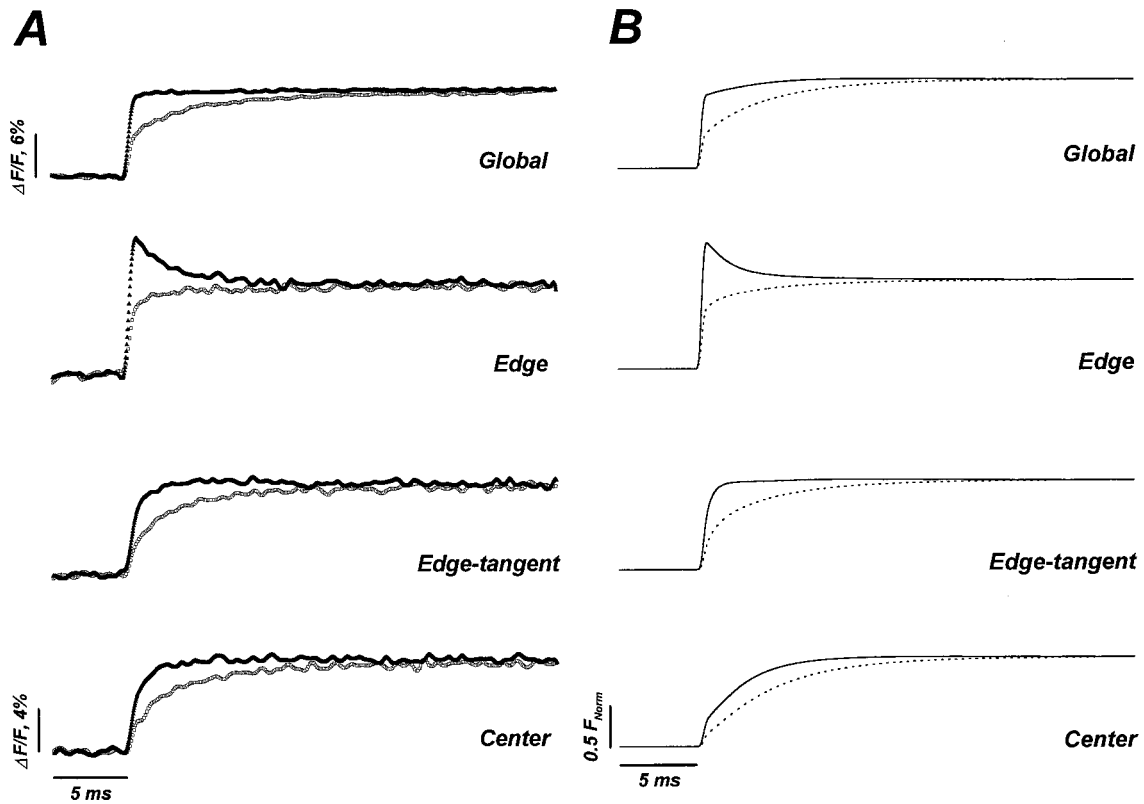
FIGURE 6 Potentiometric fluorescence transients from different illumination regions and corresponding model predictions. (*A*) In each panel, transients elicited by step pulses are plotted with open squares, and the corresponding supercharging transients are plotted with solid triangles. Illumination regions are labeled according to the nomenclature described in Materials and Methods: Global, Edge, Edge-tangent, and Center. Both traces in the Global region panel represent the average of five sweeps. All other traces were signal averaged with $n = 10$. Supercharging parameters: $\tau_1 = 1.0$ ms, 100%; $\tau_2 = 3.2$ ms, 40%; $\tau_3 = 40.0$ ms, 5%. The pulse amplitude for step and supercharging waveforms was 120 mV, applied from a holding potential of -90 mV. Fiber diameter $= 160$ μm. (*B*) Data from model simulations are presented in the same format as in *A*. Each panel superimposes model predictions in response to step ($\cdot\ \cdot\ \cdot\ \cdot\ \cdot$) and supercharging (——) pulse inputs with illumination regions as labeled (see Appendix B). Traces are normalized to a steady-state fluorescence value attained 30 ms after pulse onset. Model parameters for all panels were as follows: step size $= 120$ mV; $\tau_1 = 1.0$ ms, 100%; $\tau_2 = 3.2$ ms, 40%; $\tau_3 = 40.0$ ms, 5%; 30 units; fiber radius $= 80$ μm; $R_s = 125$ $\Omega \cdot$ cm^2; $G_L = 0.01$ S $\cdot$ cm^{-1}; $\sigma = 0.5$; $\rho = 3 \times 10^{-3}$; $\zeta = 10^{-6}$ cm; $C_w = 1.25$ μF $\cdot$ cm^{-2}; $G_w = 1.2 \times 10^{-5}$ S $\cdot$ cm^{-2}; 2-kHz 8-pole digital Bessel filter; Lorentzian illumination with 20 θ divisions. Global case: surface membrane contribution $= 33\%$. Edge case: surface membrane contribution $= 60\%$; $d = 60.0$. Edge-tangent case: surface membrane contribution $= 10\%$; $d = 60.0$. Center case: surface membrane contribution $= 10\%$; $d = 15.0$.

model simulations (Fig. 8 *B*) demonstrate features similar to the experimental data only when a large R_s value (145 $\Omega \cdot$ cm^2) is selected. When smaller R_s values are used, the model predicts that a marked fluorescence overshoot is evident early during the pulse.

Three-dimensional representations of T-system voltages

Three-dimensional graphs of T-system voltage as a function of time and radial distance further illustrate how step (Fig. 9 *A*) and supercharging (Fig. 9 *B*) waveforms assert voltage changes along the T-system when modeled as a radial cable with an access resistance. When we use a typical fiber radius (65 μm) and an R_s of 135 $\Omega \cdot$ cm^2, a step pulse causes the voltage in the outermost shell of the T-system (shell 30, Fig. 9 *A*) to rise with a rounded time course that achieves 95% of the steady-state value in $\sim$8.4 ms. At the opposite end of the T-system, the innermost shell (shell 0)

voltage rises with slightly slower kinetics because of the passive electrical conduction properties along the radial cable. The supercharging pulse, in contrast, induces a step-like voltage change in the outermost T-system shell (shell 30, Fig. 9 *B*) that reaches 95% of the steady-state value in $\sim$1.2 ms. Moreover, it can be observed that the supercharging pulse establishes steeper radial voltage gradients that dissipate more rapidly than does the step pulse.

These features are evident in grayscale contour plots of the same simulations. In the step plot (Fig. 9 *C*) there is a disperse distribution of voltages (normalized to percentage of steady-state) over time and along the T-system, suggestive of the relatively slow rise in the overall T-system potential that step pulses achieve. The supercharging pulse generates a much narrower voltage spread both in time and through the T-system (Fig. 9 *D*). This plot also illustrates that the outer three elements of the 30-element cable (approximately the peripheral 13 μm of a 130-μm-diameter fiber) attain at least 90% of the steady-state voltage in $\sim$2
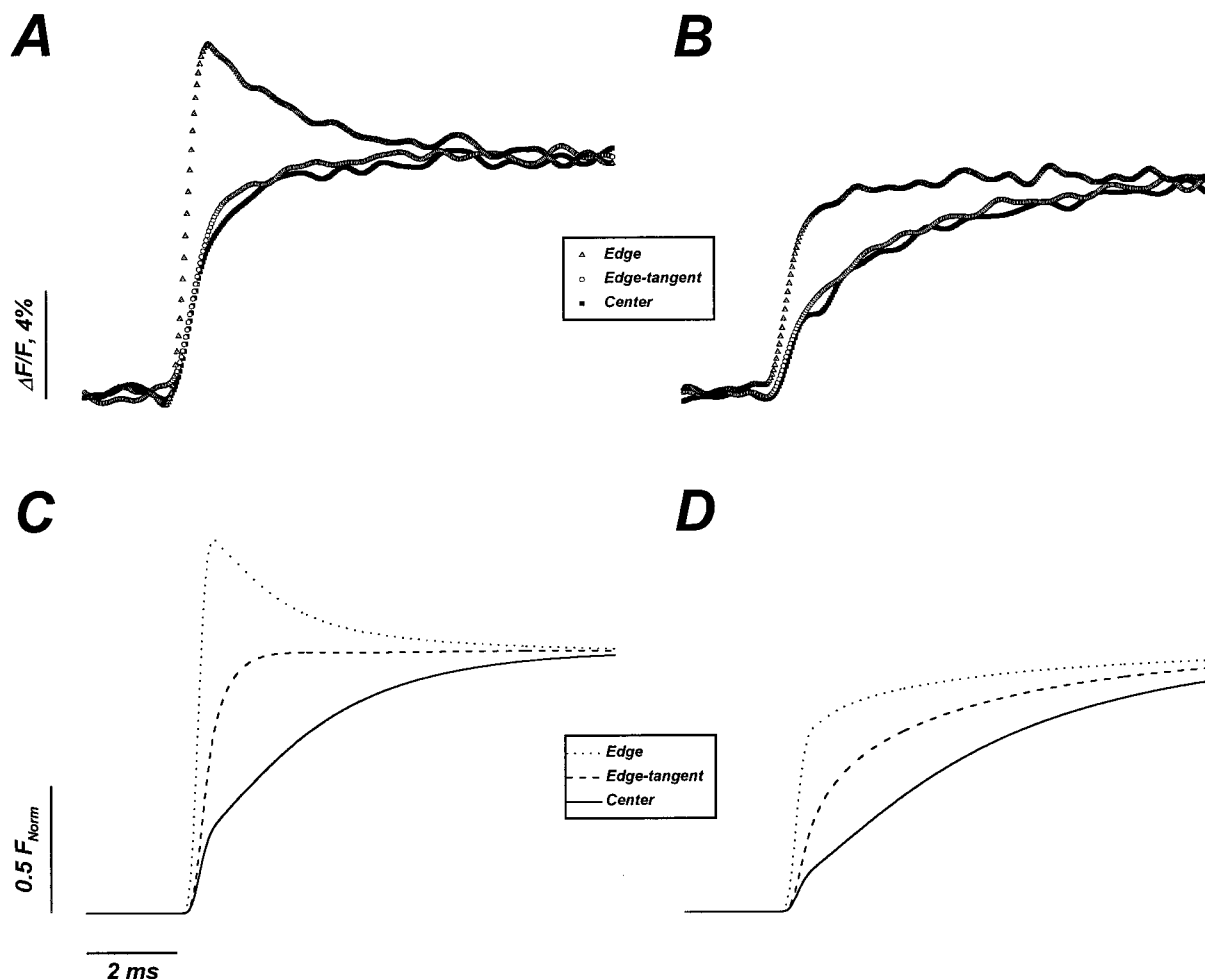
FIGURE 7   Expanded time scale kinetic comparison of regional data and model predictions. Data are plotted as points and model traces are plotted as lines: ■, ——, Center; ○, – – –, Edge-tangent; ▲, · · · · ·, Edge. (*A*) Evoked fluorescence transients in response to supercharging pulses. (*B*) Evoked fluorescence transients in response to step pulses. (*C*) Model simulation results using supercharging pulses. (*D*) Model simulation results using supercharging pulses. Traces in *A* and *B* are the same as those in Fig. 6 *A*, and the traces in *C* and *D* are the same as those in Fig. 6 *B*. Model parameters are as specified in Fig. 6 *B*.

ms in this simulation, versus ~6.6 ms for the step case (cf. Fig. 9 *C*).

DISCUSSION

This report examines the use of supercharging command pulses as an alternative to the step waveforms traditionally employed in voltage-clamp studies of skeletal muscle. Through the use of globally detected potentiometric fluorescence transients, we document that depolarization of the passive T-system is significantly accelerated when correctly tuned supercharging pulses are applied. Results obtained from localized illumination regions verify that peripheral sections of the T-system are not severely overcompensated by proper supercharging pulses, and quantitative model predictions affirm this finding. Building on earlier models of T-system electrical properties and the distributed radial cable approximation (Falk and Fatt, 1964; Falk, 1968; Adrian et al., 1969a), our model explicitly incorporates the

access resistance boundary condition (Adrian and Peachey, 1973) into its voltage calculations (Appendix A). In addition, it accounts for differences in evoked potentiometric fluorescence when illumination regions and intensities are varied (Appendix B).

Properties of di-8 ANEPPS fluorescence signals

di-8 ANEPPS is a fast styryl potentiometric indicator that has been used extensively to measure membrane voltage changes (Bedlack et al., 1992; Rohr and Salzberg, 1994). In agreement with the findings of Rohr and Salzberg (1994), this dye performed with low toxicity and minimal photobleaching, and we observed T-system membrane voltage changes with signal-to-noise ratios as high as 30:1 (2-kHz bandwidth). Typically, fluorescence changes in response to voltage clamp pulses were ~6% $\Delta F/F$ increases per 100-mV depolarization, smaller than the 10–15% changes reported by Rohr and Salzberg (1994). This difference may
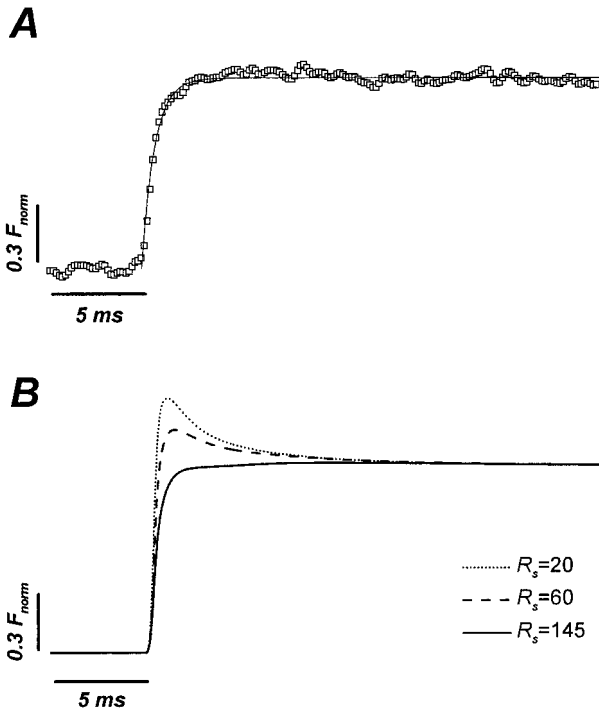
A

B

FIGURE 8 Experimental record and model predictions for Edge-tangent region evoked fluorescence. (*A*) Edge-tangent fluorescence transient (□) and single exponential function fit trace (———). Same data as in Figs. 6 *A* and 7 *A*, but normalized to the steady-state fluorescence 30 ms after the onset of the pulse. Fitting function same as in Fig. 3; $y_0 = 0$, $A = 1.0$, and $\tau = 0.7$ ms. (*B*) Normalized model simulations for Edge-tangent region illuminations. R_s was varied as indicated from 20 to 145 $\Omega \cdot cm^2$ (all other parameters are as specified for Figs. 6 *B* and 7 *B*).

be due to the lower temperature at which our studies were performed (15° versus 35°C), or to a greater contribution of baseline fluorescence from staining of nonmembrane extracellular components in our dissected fibers.

The steady-state fluorescence-voltage plot in Fig. 4 demonstrates that di-8 ANEPPS transients are scalable over a wide range of voltages applied. This result, observed in response to both supercharging and step pulses, is advantageous in that dye behavior is predictable in the voltage range tested and because the kinetics of reported fluorescence changes (e.g., Fig. 3) are not distorted by voltage-dependent nonlinearities. It also demonstrates that the T-system was rendered passive, i.e., that all significant ionic conductances were blocked.

We did not detect the nonlinear electrostatic potential changes previously reported for the absorbance potentiometric dye WW375 (Heiny and Jong, 1990; Jong et al., 1997) in our experiments. Such changes should have manifested themselves at voltages higher than −50 mV, but are not obvious in Fig. 4 for either the step or supercharging case. This discrepancy may reflect intrinsic differences in the mechanisms through which these dyes report membrane potential changes or the presence/absence of voltage-dependent processes secondary to dye staining.

Approaches to supercharging

The rate limitations in charging the passive skeletal muscle T-system with step voltage-clamp command pulses have been recognized both in theory (Falk and Fatt, 1964; Falk, 1968; Adrian et al., 1969a; Adrian and Peachey, 1973; Ashcroft et al., 1985; Simon and Beam, 1985) and experimentally (Vergara and Bezanilla, 1981; Heiny and Vergara, 1982; Heiny and Vergara, 1984; Ashcroft et al., 1985; Simon and Beam, 1985). These limitations arise partially because of the intrinsic cable properties of the T-system, but also because of a large access resistance separating the extracellular fluid from the T-system lumen (Adrian and Peachey, 1973). At the inception of the current methodology, we proposed that a properly designed supercharging command waveform should readily compensate for the voltage drop across the access resistance and ensure that the intended test voltage is applied at the edge of the T-system cable (Vergara and Kim, 1997; Kim and Vergara, 1998).

To achieve a quasistep in the T-system potential, we explored several modifications of the standard voltage-clamp methodology, including 1) step pulses in combination with a series resistance compensation pathway that involved positive feedback of a fraction of the measured total ionic current into the voltage command amplifier, and 2) de novo command pulse generation using an analog electronic circuit that summed a voltage step with one, two, or three adjustable exponential decay phases. The first option is analogous to the approach used previously to measure (and compensate for) the series resistance that arises from the Schwann cell sheath in the squid giant axon (Salzberg and Bezanilla, 1983). However, this method was unsatisfactory because the surface membrane capacitive current component dominated the feedback signal and destabilized the voltage clamp. Even when the current feedback signal was low-pass filtered at corner frequencies as low as 500 Hz, we were unable to provide adequate boosting of T-system depolarization without introducing voltage oscillations. The second system is strategically similar to that used by Armstrong and Chow (1987) to compensate pipette series resistances in whole-cell patch-clamp experiments, but was extended to incorporate multiple exponential phases rather than one. Although stable, it was inconvenient because τ and A values could not be uniquely quantified. Based on these results, we enhanced the technique by adding digital control to generate the supercharging waveforms according to precise formulas (see Materials and Methods and Appendix A).

Using the radial cable model (Adrian et al., 1969a) with an access resistance (Adrian and Peachey, 1973), a straightforward analysis (data not shown) predicts that under voltage-clamp conditions, the command waveform required to implement a voltage step, V, at the cable's edge is given by

$$V_{com}(T) = V\left(1 + \frac{2\bar{G}_L R_S}{a} \sum_{n=1}^{\infty} \frac{\alpha_n^2 \exp - [(\nu^2 + \alpha_n^2)]T}{\nu^2 + \alpha_n^2}\right) \quad (1)$$
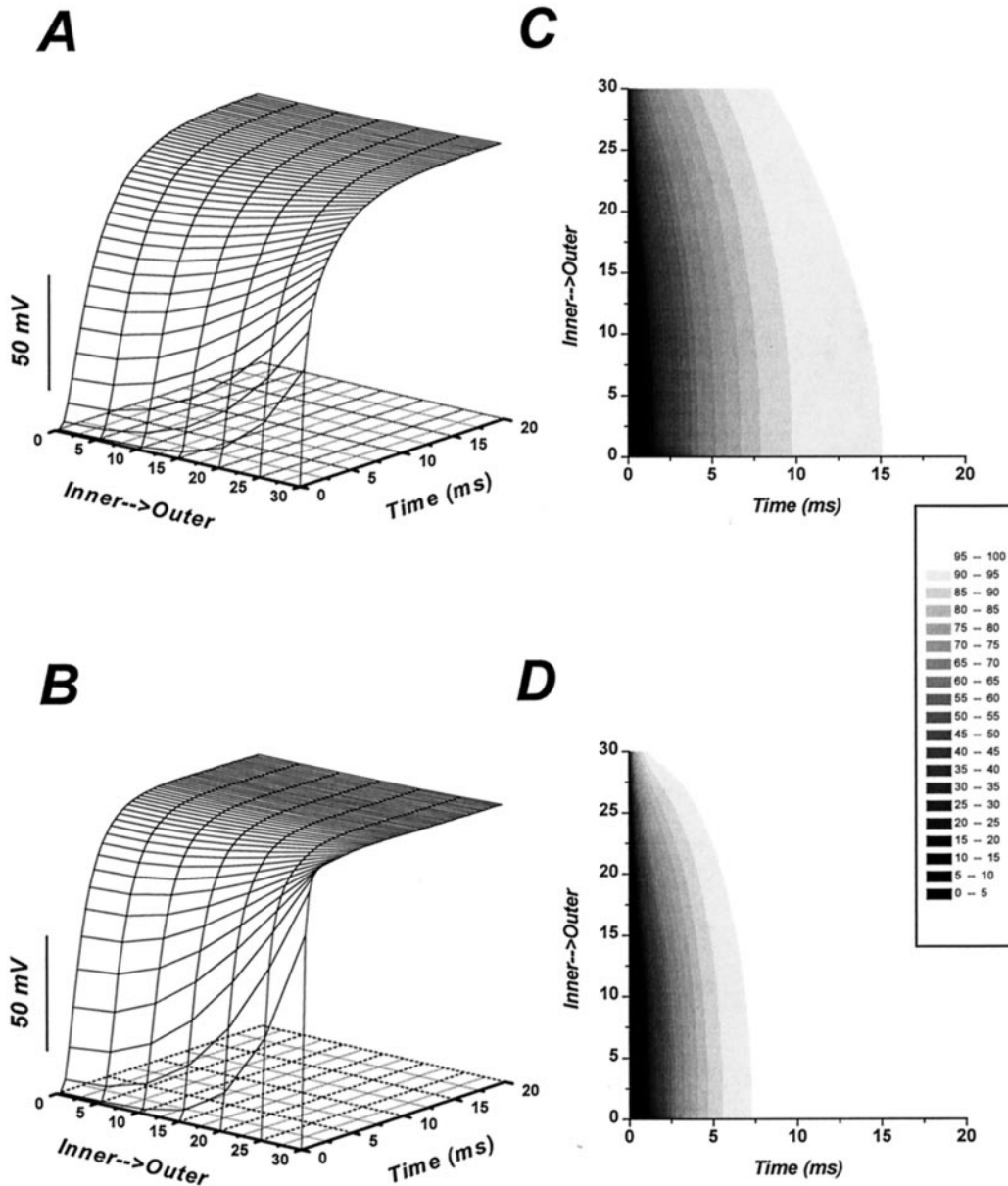
FIGURE 9   Orthographic and contour plots of simulated early T-system depolarization events. (*A*) Twenty-millisecond step pulse simulation. (*C*) Contour gray scale plot of the simulation in *A*. (*B*) Twenty-millisecond supercharging pulse simulation. (*D*) Contour gray scale plot of the simulation in *B*. The common legend for *B* and *D* expresses units as a percentage of steady-state voltage, 120 mV. Model parameters are as follows: step size = 120 mV; $\tau_1 = 1.1$ ms, 81%; $\tau_2 = 3.2$ ms, 22%; $\tau_3 = 40.0$ ms, 1%; 30 units; fiber radius = 65 μm; $R_s = 135 \ \Omega \cdot \text{cm}^2$; $G_L = 0.01 \ \text{S} \cdot \text{cm}^{-1}$; $\sigma = 0.5$; $\rho = 3 \times 10^{-3}$; $\zeta = 10^{-6}$ cm; $C_w = 1.25 \ \mu\text{F} \cdot \text{cm}^{-2}$; $G_w = 1.2 \times 10^{-5} \ \text{S} \cdot \text{cm}^{-2}$.

where α_n's are the positive roots of $J_0(\alpha) = 0$, and J_0 is a Bessel function of the first kind. All other variables are as defined in Appendix A.

The infinite sum of exponentials specified by Eq. 1 is impractical to generate during an experiment, but we found that three exponentials could adequately achieve a reasonable degree of compensation.

Global transient characteristics and compensation criteria

In both step and supercharging cases, global transients document that the average T-system potential changes in a

manner that is distinctly unlike the applied command waveform. In Fig. 3 *A*, T-system fluorescence transients evoked by step pulses exhibit an early jump in fluorescence (more obvious in Fig. 3 *C*) that is only a fraction of the steady-state amplitude, and then a slower, pseudoexponential rise to the final value. Fig. 3 *B* shows that supercharging pulses can boost the kinetics of T-system depolarization noticeably. Using τ's from single exponential fits as quantitative approximations of rates of fluorescence change, we found that global supercharging-evoked transients reached 95% of steady state almost an order of magnitude faster than their step counterparts (1.5 ms versus 14.6 ms). The 95% charg-

ing time we report for step pulses is similar to the $\sim$15–20 ms observed in previous studies using several potentiometric indicators (Vergara and Bezanilla, 1981; Heiny and Vergara, 1982, 1984; Heiny et al., 1983; Ashcroft et al., 1985; Jong et al., 1997). However, it is significantly slower than the 3.7 ms reported by Heiny and Jong (1990) for the absorbance dye WW375. The discrepancy exists despite the use of similar fibers and solutions. Because WW375 exhibits prominent wavelength-dependent dichroic absorbance properties that can bias signals toward surface membrane contributions (Vergara and Bezanilla, 1981; Heiny and Vergara, 1984), it is possible that the use of unpolarized light (Heiny and Jong, 1990) in combination with uncertainties in fiber geometry may have emphasized such effects. On the other hand, the slower WW375 transients reported later by the same authors (Jong et al., 1997) are similar to ours.

Intrinsic to the design of an optimally tuned waveform was a tradeoff between boosting depolarization speed and the potential hazard of gross T-system overcompensation. The quasistep criteria were selected as a conservative performance estimate while still allowing reasonable acceleration over step pulse depolarization. As shown in Fig. 5, significant overcompensation is only seen when extraordinarily large command waveforms are applied. The parameters for such command pulses lie well outside the typical range of values (see Table 1), so that cautious parameter selection avoids severe compensation errors in the vast majority of experiments. However, with $\Delta F/F_0$ values ranging from 4% to 8% per 100 mV, subtle errors in compensation may be lost in the baseline noise of the detected fluorescence.

The average parameters used to elicit well-tuned quasisteps in global T-system fluorescence (Table 1) were reasonably uniform in the values of τ_1-τ_3 necessary. This was not surprising because of the relative consistency of T-system architecture between fibers of different sizes and capacitances (Peachey, 1965b; Eisenberg, 1983). Although amplitude values varied considerably, fibers of similar diameter dissected from the same muscle tended to respond similarly to a given set of supercharging parameters. Blind application of identical parameter sets (τ's and A's) in these cases consistently produced transients that satisfied the optimization criteria. The overall trend suggested that larger fibers required more amplitude contribution than smaller fibers, especially A_2, but statistical variability in the pooled data suggests that several other experimental factors may be involved. For example, variability in grease seal resistance, fiber ellipticity, and the amount of connective tissue overlying the sarcolemma all may alter the performance of the voltage clamp in charging the T-system and hence affect the evoked fluorescence. It is plausible that slight inconsistencies in these factors can result in the parameter variations observed. For example, if a change in connective tissue density surrounding a dissected fiber were to effectively increase the access resistance term to the modeled T-system from 110 to 150 $\Omega \cdot cm^2$, the A_1 and A_2 terms would require

changes on the order of 10–40% (keeping τ_1-τ_3 and other parameters constant) to achieve an equivalently performing supercharging waveform. Despite the uncertainties, the parameter ranges and average values presented in Table 1 furnish reasonable guidelines for conservative use of the supercharging method as presented.

It should be clarified that our τ_1 and τ_2 are not meant to correspond to individual components of the infinite sum of Eq. 1; instead they probably represent groups of terms in the sum. It follows that the amplitudes A_1 and A_2 are weighting factors for the terms grouped by τ_1 and τ_2. Adrian et al. (1969a) derived a theoretical approximation of a dominant "final" time constant, τ_f, that describes the slow phase of the transient current required to establish a step change in potential at the edge of the T-system cable. Interestingly, the calculated τ_f would be 1.7 ms for a typical fiber (parameters identical to those used in Fig. 9), a value intermediate to the experimental averages for τ_1 and τ_2 (1.0 and 3.4 ms, respectively). Another prediction from Eq. 1 is that the amplitude coefficient of τ_f should be $\sim$62% of the applied V (in the case where $R_s = 135 \ \Omega \cdot cm^2$). This value is also intermediate to the average values for A_1 and A_2 (87% and 53%, respectively). Experimentally, however, using a single exponential boosting function never resulted in optimal compensation. Thus it may be the case that the combination of τ_1 and τ_2 is an adequate weighted approximation of the most influential terms of the sum in Eq. 1.

Why was it necessary to use a third supercharging component (i.e., A_3 and τ_3)? Its minor contribution ($\sim$5%) was essential for boosting a creeping phase in the T-system fluorescence signals. Control records indicate that for the short illumination periods used ($<$1 s), fluorescence bleaching effects were negligible. Furthermore, fluorescence decreases and increases evoked by depolarizing and hyperpolarizing pulses, respectively, both benefited from incorporating τ_3 and A_3. The compensatory effect of the third exponential factor was generally more pronounced in those experiments where larger nonspecific leak currents were detected during voltage-clamp pulses.

The satisfactory results obtained using only three time constants do not preclude the possibility that future use of more complex waveforms may further optimize the supercharging protocol. For example, better approximations of the theoretical solution in Eq. 1 may be achieved by incorporating additional exponential terms.

Regional illumination fluorescence transients

The contrasts between Edge and Edge-tangent localized illumination transients more clearly define how the access resistance transforms voltages between surface and T-system membrane. Edge region supercharging traces (Fig. 6 A) are characterized by a prominent overshoot followed by a decay to steady-state fluorescence. These features strongly resemble the applied waveform, and are expected results, considering the relative amounts of surface and T-system

membrane illuminated. If we assume that the fiber is cylindrical with a radius of 80 μm (per the fiber in Fig. 6 *A*), and that the illumination beam approximates a cylinder (see Fig. 12, Appendix B) with a radius of 30 μm passing through the fiber 15 μm from the edge, the Edge region (see schematic in Fig. 1 *B*) corresponds to a peripheral ~5% of the global illumination fiber volume. It can be inferred that the fluorescence signal from Edge illumination is dominated by surface membrane potential changes, with only a small contribution from the peripheral T-system.

Because the surface membrane potential is supercharged as a result of the applied waveform, we must ask the question: Do supercharging pulses severely overcompensate the peripheral T-system as well? Edge-tangent supercharging transients (Fig. 6 *A*) provide a negative response, demonstrating an early fluorescence jump without overshoot, followed by a slower rise to steady-state in ~2 ms. Applying a calculation analogous to the one above, but assuming full overlap and an illumination beam cylinder radius of 15 μm, the Edge-tangent region (see schematic in Fig. 1 *B*) illuminates a volume near the edge of the fiber that is only 6% of the globally illuminated volume. A minor surface membrane contribution remains, but the dominant source of the emitted fluorescence transients is the outermost elements of the T-system. The differences between transients from the Edge and Edge-tangent regions concur with the proposal of Adrian et al. (1973) that morphological barriers between surface membrane and T-tubules (Peachey, 1965a; Zampighi et al., 1975) are responsible for the considerable electrical isolation of these membrane systems.

Regional illumination model predictions

Our model should verify the experimental data by predicting fluorescence transients that reflect the behavior of the electrical transfer function between surface and T-tubule. The parallels between the traces in Fig. 6, *A* and *B*, indicate that the effects of supercharging pulses are compatible with an established theoretical representation of the T-system (Adrian et al., 1969a; Adrian and Peachey, 1973; Ashcroft et al., 1985). In both Edge and Edge-tangent cases, modeled traces agreed well with experimental records. The 60% weighting of surface contribution in the Edge simulations is consistent with the high proportion of surface membrane with respect to T-system in the illumination volume. Similarly, the 10% weighting factor used in the Edge-tangent case reflects the lower proportion of surface illuminated.

Surprisingly, the Global and Center experimental data were less adequately predicted in model simulations. This is noticeable in the necessarily relatively heavy surface weighting of the Global traces in Fig. 6 *B* (33%) and in the slower kinetics of Center traces in Figs. 6 *B*, 7 *C*, and 7 *D* (cf. data traces in Figs. 6 *A*, 7 *A*, and 7 *B*). These discrepancies are likely of common origin, and may be due to potential differences between Center region model predictions for fluorescence and the actual detected Center region

fluorescence. As defined in Appendix B, the computer algorithm calculates Center region fluorescence by defining an illumination profile that favors contributions from inner T-system cable elements (Fig. 13 *B*). The simulated Center traces show kinetics perceptibly slower than Edge-tangent or Edge traces, as expected from cable theory, but this effect is less prominent in the experimental data. One possible source of this deviation is the known ellipticity of muscle fibers (Blinks, 1965; Heiny and Vergara, 1984), which our model does not consider. A fiber with an elliptical rather than circular cross section has an increased surface-to-volume ratio that may result in a heavier emphasis on fluorescence changes arising from more peripheral regions of the T-system and the surface membrane. For example, in a fiber of radius *a*, an elliptical cross section with an eccentricity of 0.5 gives a surface-to-volume ratio that changes as ~3.2/*a* versus 2/*a* for a circular cross section. Alternatively, the more central vicinities of the T-system may be less thoroughly stained and, as a result, may contribute less to the observed fluorescence signals. Although confocal images (Fig. 1 *A*) do not appear to support this hypothesis qualitatively, we cannot discount the possibility that such inhomogeneities may exist.

In simulations designed to test these experimental possibilities, we eliminated the contributions of the innermost 10–15 cable segments and found that subsequent fits to experimental Global transients (data not shown) were improved such that the surface membrane contribution could be diminished to a more reasonable value (<15%). Experiments using confocal techniques and three-dimensional image reconstruction may be necessary to further investigate these hypotheses.

It may be argued that a high luminal conductivity provides another conceivable explanation for the kinetic closeness of Edge-tangent and Center transients (Fig. 6 *A*). In this scenario, abundant fixed charges in the T-system membranes may increase luminal conductivity to well above the bulk solution. To test this reasoning, we ran simulations with values of G_L significantly larger than the measured $0.01 \text{ S} \cdot \text{cm}^{-1}$ of the external solution. With the conductivity at more than five times that of normal Ringer's solution ($G_L > 0.05 \text{ S} \cdot \text{cm}^{-1}$), it was possible to attain relatively uniform cable behavior such that voltage changes in the outermost and innermost regions of the T-system showed comparable kinetics. Under these conditions, however, the slower rising phases of modeled Edge-tangent transients were in poor agreement with those observed experimentally. To match these time courses, it was necessary to adjust τ_1-τ_3 and A_1-A_3 to values inconsistent with those used during experiments. Hence we do not favor this hypothesis as the only explanation.

It should be emphasized that the Edge-tangent controls (both data and model; see Figs. 6–8) were critical to confining the value of R_s and validating the relevance of Global illumination transients. Earlier work investigating the access resistance with potentiometric dyes (Heiny et al., 1983; Ashcroft et al., 1985) did not employ regional detection and

was not subject to the concomitant constraints. In particular, the absence of an overshoot in the early phase of Edge-tangent region evoked fluorescence (Fig. 8 *A*) is inconsistent with model predictions using a small access resistance (Fig. 8 *B*) and implies that a large R_s isolates the T-tubule from the surface membrane. In addition, the similarity between Global and Edge-tangent rising kinetics ($\tau = 0.5$ versus $\tau = 0.7$ ms, respectively) in response to supercharging pulses indicates that Global signals do not significantly misrepresent the voltage changes in the peripheral T-system. This result is encouraging because Global signals have better signal-to-noise ratios and are far easier to obtain than more localized signals.

Voltage distribution in the T-system cable

The three-dimensional plots in Fig. 9 illustrate the kinetic constraints that an access resistance places on charging the passive T-system cable and how supercharging compensates for these limitations. An important consequence of the voltage drop across an access resistance is that a step voltage pulse applied at the surface changes the membrane potential slowly, even at the outermost element of the T-system (Fig. 9, *A* and *C*). Passive cable electrical properties further slow the depolarization time course at the inner regions of the T-system such that they reach 95% of the steady-state voltage ~15 ms after the onset of the step command pulse. The effect of the supercharging command pulse is to compensate for the inevitable voltage drop and establish the desired test voltage at the edge element as rapidly as possible. As shown in Fig. 9, *B* and *D*, this scenario not only allows a fast voltage change in the outer regions, but also accelerates depolarization kinetics in the entire T-system cable. In these simulations, supercharging boosts the depolarization rate by a factor of ~7 at the outermost element and by a factor of ~2 at the innermost element. Our data agree qualitatively with these findings but suggest that the kinetic improvement may be even greater.

The supercharging plots in Fig. 9, *B* and *D*, portray the outcome of simulations whose optimization criterion sought to impose a voltage step at the outermost element of the T-system cable by using the waveform recipe delineated in Appendix A. It can be seen that through supercharging, the depolarization achieved at the outermost cable element is markedly accelerated compared to the step-induced depolarization (Fig. 8 *A*) but still falls short of the ideal instantaneous step change. As mentioned previously, the use of more complex waveforms may further improve our ability to rapidly establish changes in potential.

Radial cable model electrical parameters

To account for the values A_1-A_3 required to impose a quasistep in the Global and Edge-tangent transients, it was necessary to include significant access resistance values in model simulations. Our range of 110–150 $\Omega \cdot cm^2$ is in

good agreement with the 150 $\Omega \cdot cm^2$ used to isolate surface and T-system membranes for the purpose of reconstructing the propagated action potential in muscle fibers (Adrian and Peachey, 1973). However, our values are larger than the 20–50 $\Omega \cdot cm^2$ previously reported in frog skeletal muscle with model fits to absorbance potentiometric dye transients (Heiny et al., 1983; Ashcroft et al., 1985). This difference may be due to the fact that the global region optical data in these earlier studies may have been significantly biased toward surface membrane or more peripheral T-system kinetics because of the dichroic properties of the indicators used. In addition, their use of solutions with smaller effective G_L (0.0073 $S \cdot cm^{-1}$ versus our 0.01 $S \cdot cm^{-1}$) favors smaller access resistance values in model simulations (Kim and Vergara, unpublished observations). The current study also provides a more rigorous assessment of R_s because of the regional illumination schemes in both model and experiments, and because of the requirement that the model satisfy both step and supercharging data.

The 60 $\Omega \cdot cm^2$ access resistance used preferentially to fit rat skeletal muscle charge movements (Simon and Beam, 1985) is also smaller than our values. However, these authors also note that when the surface membrane charge is included, it is necessary to use a larger value for the access resistance (100 $\Omega \cdot cm^2$), which is in better agreement with our values. Finally, impedance analysis studies of frog skeletal muscle fibers (Valdiosera et al., 1974) found access resistance values of ~20–130 $\Omega \cdot cm^2$ for fibers bathed in Ringer solutions of varying tonicities (normal to 2.5 times hypertonic with sucrose).

All other radial cable model parameter values (see Appendix A and figure legends) are similar to those used in previous studies (Adrian et al., 1969a; Adrian and Peachey, 1973; Heiny et al., 1983; Ashcroft et al., 1985; Simon and Beam, 1985), with two exceptions. First, we used a G_w of 1.2×10^{-5} $S \cdot cm^{-2}$ derived from model fits to the steady-state leak observed in our current records. This value is lower than the 5.0×10^{-5} $S \cdot cm^{-2}$ used by Adrian et al. (1969a) and the 3.2×10^{-5} $S \cdot cm^{-2}$ used by Simon and Beam (1985). Second, we preferred to use a C_w of 1.25 $\mu F \cdot cm^{-2}$ instead of the usual 1.0 $\mu F \cdot cm^{-2}$. This higher value provided better agreement with experimentally required values for A_1-A_3, the kinetics of fluorescence transients evoked in response to step pulses, and the total fiber capacitance observed.

Physiological implications

When considered in the context of skeletal muscle E-C coupling, the data presented in this paper emphasize that the results from studies employing step command pulses to investigate voltage-dependent mechanisms involving the T-system (e.g., Ca^{2+} release and charge movements) reflect the rate-limited time course of depolarization shown. As reported previously, supercharging pulses elicit Ca^{2+} release fluorescence transients and charge movements (Ver-

gara and Kim, 1997; Kim and Vergara, 1998) that display kinetic accelerations paralleling the boost demonstrated here for membrane potential changes. An important question remaining is, can supercharging pulses depolarize the passive T-system at a rate comparable to that seen physiologically during a Na^+ conductance-dependent action potential? The superimposed global fluorescence traces in Fig. 10 *A* illustrate that this is possible. Whereas the supercharging transient and the action potential transient (global traces, obtained from different fibers) rise at similar rates, the step transient is noticeably slower (for comparison, see also Fig. 3 *E*). Furthermore, in response to the step pulse, the T-system potential continues to change over the entire time interval plotted, whereas in response to the supercharging pulse and the action potential, the depolarization reaches a maximum in approximately the first 2 ms.
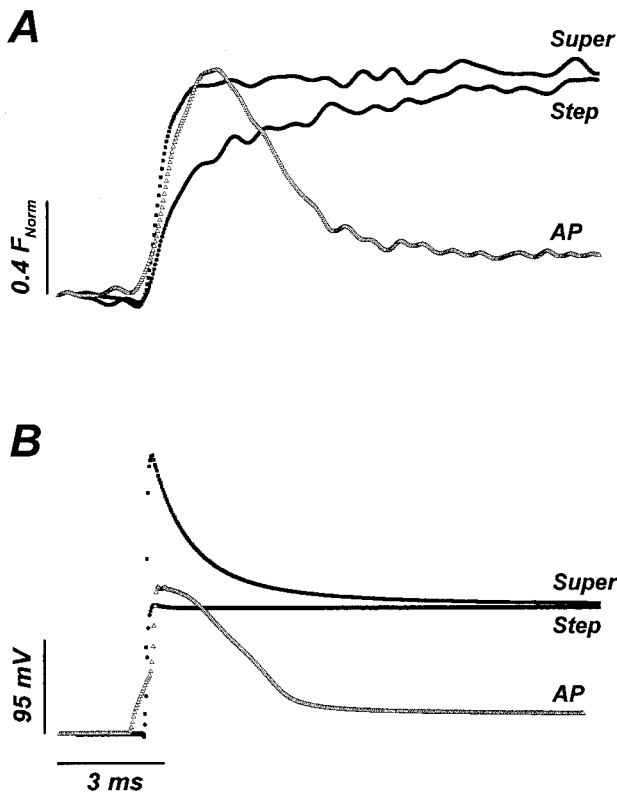

A

B

FIGURE 10   Scaled comparison of action potential and voltage-clamp transients. (*A*) Superimposed fluorescence transients obtained in response to supercharging (■) and step (●) voltage-clamp pulses, and to an action potential (△). (*B*) Recorded voltage traces corresponding to the transients in *A*. Symbols are as in *A*. The action potential traces in *A* and *B* were left-shifted by 0.5 ms, the length of the current injection stimulus. Voltage-clamp pulses were 120 mV in amplitude applied from a holding potential of −90 mV. The action potential fluorescence trace (single sweep) in *A* was normalized to its peak amplitude (5% $\Delta F/F$), and the voltage-clamp transients (signal averaged, $n = 4$) were normalized to the steady-state fluorescence (8% $\Delta F/F$) taken as the average of values during the last 5 ms of the pulse. The electrical traces in *B* were digitally filtered with a 10-kHz FFT algorithm. Fiber diameters were 105 μm for the action potential experiment and 138 μm for the voltage-clamp experiment. Supercharging parameters: $\tau_1 = 1.0$ ms, 100%; $\tau_2 = 3.2$ ms, 30%; $\tau_3 = 40.0$ ms, 5%;

It must be considered that the acceleration provided by supercharging pulses, although considerable, may still not be kinetically optimal to investigate the rapid signal transduction mechanisms of E-C coupling at T-SR junctions throughout the T-system. Nonetheless, even in the current implementation, there exist regions of the T-system (e.g., the peripheral 10%) where supercharging pulses can establish fast voltage changes such that E-C coupling processes can be probed without the kinetic penalties imposed by step pulses.

APPENDIX A: NUMERICAL INTEGRATION OF THE RADIAL CABLE MODEL EQUATIONS WITH ACCESS RESISTANCE

Equations and parameters

Fig. 11 shows a schematic diagram of the equivalent circuit used to represent the passive electrical properties of a muscle fiber of radius *a*. Following the assumptions of Adrian and Peachey (1973), the lumen of the T-tubules is separated from the extracellular fluid by an access resistance (R_s, in $\Omega \cdot cm^2$).

According to Adrian et al. (1969a), the partial differential equation that governs the radial and time (*t*)-dependent changes in T-tubule potential, $u(r, t)$ in response to potential changes at the boundary is

$$\frac{\partial^2 u}{\partial R^2} + \frac{1}{R}\frac{\partial u}{\partial R} = \nu^2 u + \frac{\partial u}{\partial T}$$

Following these authors' nomenclature, $R = r/a$, $T = \bar{G}_L t/(\bar{C}_w a^2)$, and $\nu = a\sqrt{\bar{G}_w/\bar{G}_L}$. The parameters $\bar{C}_w$ and $\bar{G}_w$ are the capacitance (in $\mu F \cdot cm^{-3}$) and conductance (in $S \cdot cm^{-3}$) of the tubular membrane per unit volume of muscle fiber, respectively, and $\bar{G}_L$ is the effective radial conductivity (in $S \cdot cm^{-1}$). If ρ is the fraction of the total muscle volume occupied by T-tubules, σ is a tortuosity factor, and ζ is the volume-to-surface ratio of the T-tubules,

$$\bar{C}_w = C_W \rho/\zeta$$

$$\bar{G}_w = G_W \rho/\zeta$$

$$\bar{G}_L = G_L \rho \sigma$$

where C_w and G_w are the T-tubule's membrane capacitance (in $\mu F \cdot cm^{-2}$) and conductance (in $S \cdot cm^{-2}$) per unit surface membrane of the muscle fiber, and G_L is the specific T-tubule lumen conductivity (in $S \cdot cm^{-1}$).

For the numerical integration of the radial cable equation, the T-system elements are approximated to be arranged in a series of isopotential concentric shells (s_i, with *i* ranging from 0 to *n*), each with voltage u_i (Adrian and Peachey, 1973). Most of the simulations in this paper were obtained with $n = 30$ shells. A higher number of concentric annuli did not significantly alter the theoretical predictions.

At a given time, *j*, the finite differences approximation for the spatial dependence in the partial differential equation for an arbitrary cable element with voltage $u_{i,j}$ is

$$\frac{\partial^2 u}{\partial R^2} + \frac{1}{R}\frac{\partial u}{\partial R} \rightarrow \frac{1}{2i(\Delta R)^2}$$

$$\cdot \{(2i + 1)u_{i+1,j} - 4iu_{i,j} + (2i - 1)u_{i-1,j}\}$$

where ΔR is the normalized distance between shells. The T-tubule cable is assumed to be sealed at the center of the muscle fiber, and the approxi-
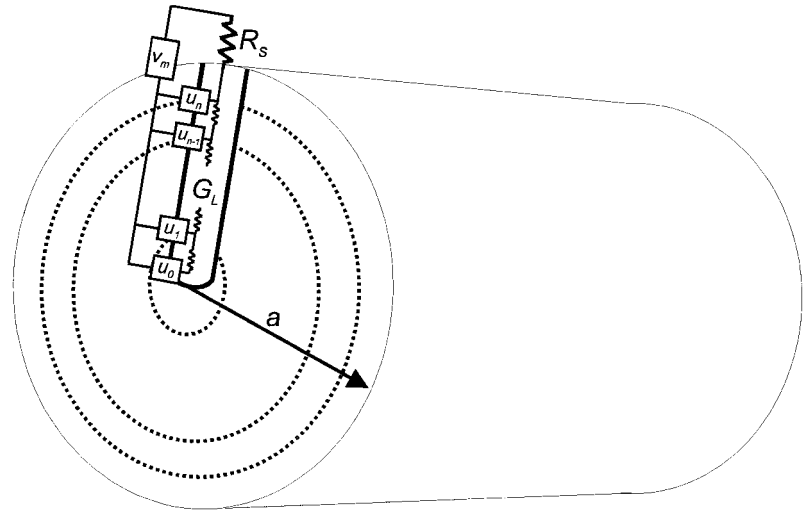
FIGURE 11   Equivalent circuit diagram of the distributed cable model.

mation used to calculate u_0 is

$$\frac{\partial^2 u}{\partial R^2} + \frac{1}{R}\frac{\partial u}{\partial R} \rightarrow \frac{4}{(\Delta R)^2}(u_{1,j} - u_{0,j})$$

The finite differences approximation for the time dependence in the partial differential equation for an arbitrary cable element with voltage $u_{i,j}$ is

$$\frac{\partial u}{\partial T} \rightarrow \frac{u_{i,j+1} - u_{i,j}}{\Delta T}$$

where ΔT is the dimensionless time interval. Rearranging the external boundary condition equation of (Adrian and Peachey, 1973) gives

$$\left(\frac{\partial u}{\partial R}\right)_{R=1} = \frac{V_{COM}(t) - u_n}{aR_s\bar{G}_L}$$

The finite differences approximation for this boundary condition is given by

$$\frac{u_{n,j} - u_{n-2,j}}{2\Delta R} = \frac{V_{COM} - u_{n,j}}{aR_s\bar{G}_L}$$

Integration

Using an implicit Crank-Nicolson algorithm (Crank and Nicolson, 1947; Gerald, 1978), a final finite difference equation for an arbitrary annulus i is obtained:

$$X \cdot \frac{(2i+1)}{4i} \cdot u_{i+1,j+1} - (X+1) \cdot u_{i,j+1} + X \cdot \frac{(2i-1)}{4i} \cdot u_{i-1,j+1}$$

$$= -X \cdot \frac{(2i+1)}{4i} \cdot u_{i+1,j} + (\Delta T \cdot v^2 + X - 1) \cdot u_{i,j}$$

$$- \frac{(2i-1)}{4i} \cdot u_{i-1,j}$$

in which $X = \Delta T/R^2$. This is a recursive formula allowing the calculation of $u_{i,j+1}$ at a time interval ΔT after $u_{i,j}$. The system of tridiagonal coefficient matrices was solved using a LU decomposition algorithm (Gerald, 1978).

Similarly for the outermost disk segment n, the Crank-Nicolson expansion gives

$$-\left\{1 + X\left[1 + \frac{(2n+1)}{4n^2 \cdot RG}\right]\right\} \cdot u_{n,j+1} + X \cdot u_{n-1,j+1}$$

$$= -X \cdot \frac{(2n+1)}{2n^2 \cdot RG} \cdot V_{COM} + \left\{\Delta T \cdot v^2 + X\left[1 + \frac{(2n+1)}{4n^2 \cdot RG}\right] - 1\right\}$$
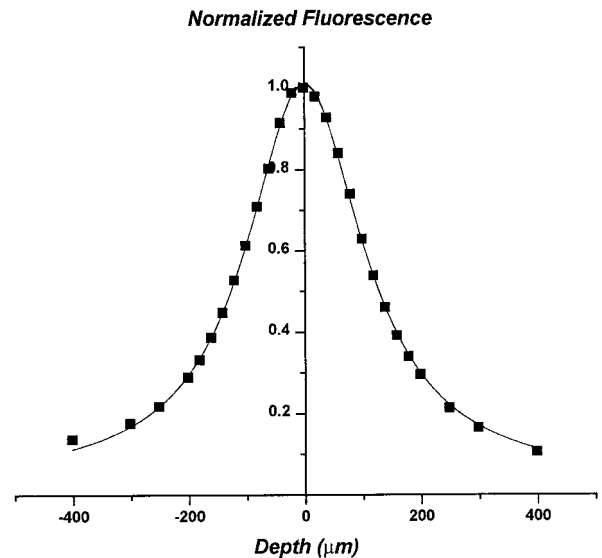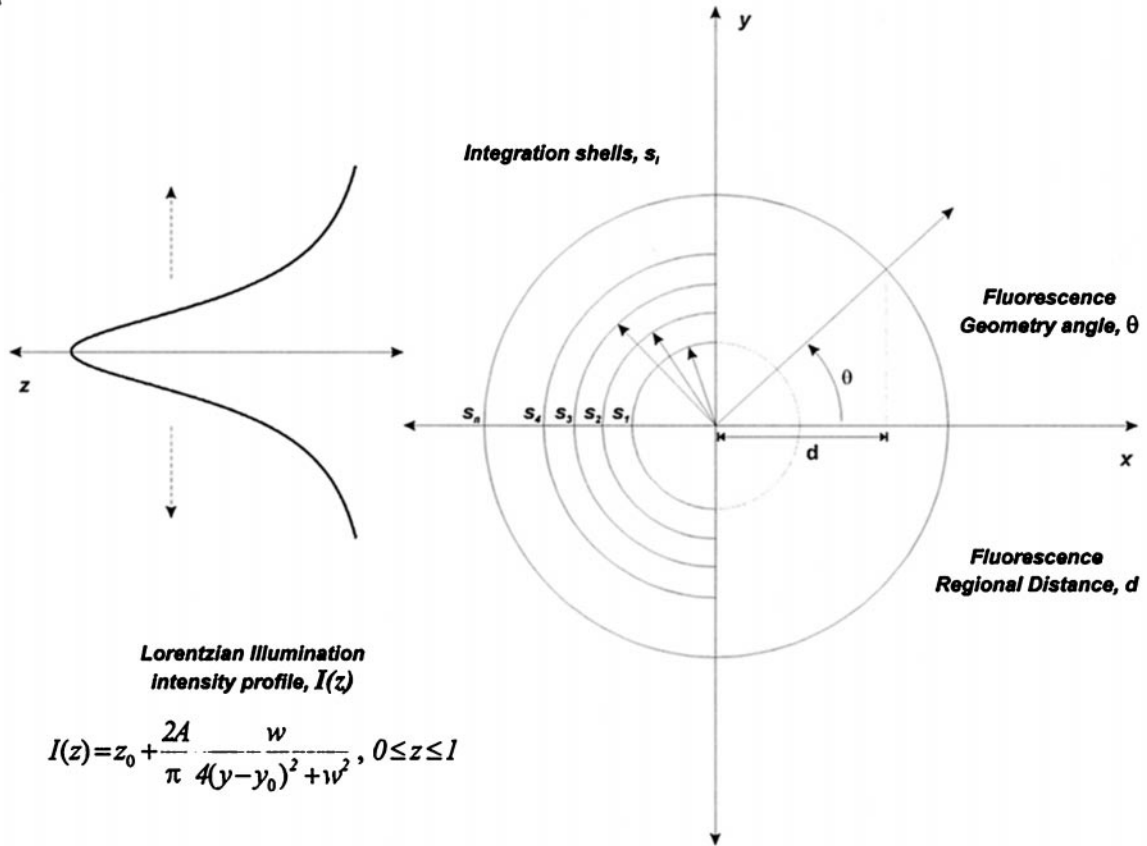
$$\cdot u_{n,j} - X \cdot u_{n-1,j}$$

FIGURE 12   Fluorescence intensity-depth profile for the 20× objective. Data points represent normalized rhodamine-G fluorescence detected from a custom-made microcuvette with a solution chamber that was 10 μm thick. The continuous line is the fitted Lorentzian function of the form
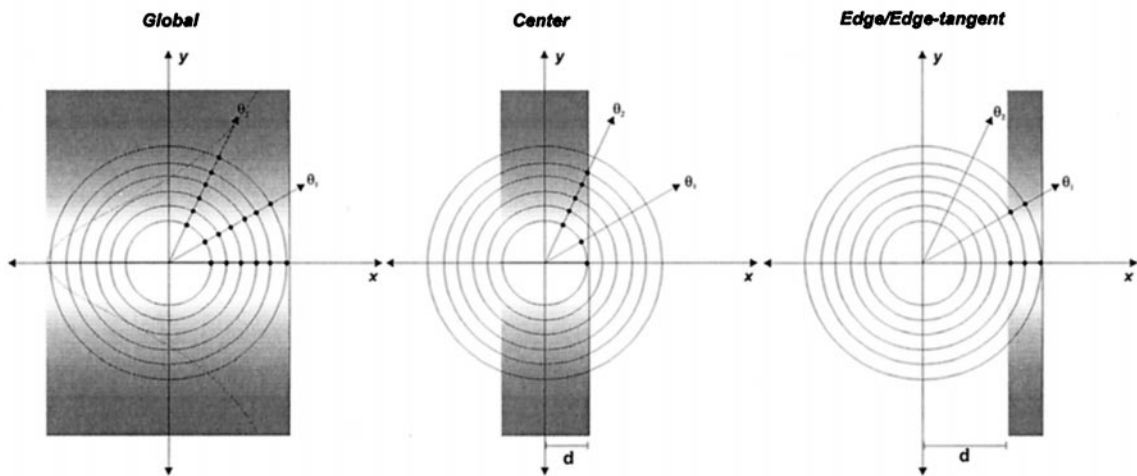
$$y = y_0 + \frac{2A}{\pi}\frac{w}{4(x - x_c)^2 + w^2}$$

$y_0 = 0.02$ normalized fluorescence units, $A = 378.72$ μm, $x_c = 0$, and $w = 245.54$ μm.

A

Integration shells, s_i

Fluorescence
Geometry angle, θ

Fluorescence
Regional Distance, d

S_n S_4 S_3 S_2 S_1

d

Lorentzian Illumination
intensity profile, $I(z)$

$$I(z) = z_0 + \frac{2A}{\pi} \frac{w}{4(y-y_0)^2 + w^2}, \ 0 \le z \le 1$$

B

Global   Center   Edge/Edge-tangent

$$\theta_j = \frac{2\pi j}{n}, \ n = \text{\# of } \theta \text{ divisions}$$

FIGURE 13 Schematic diagrams of illumination algorithm implementation. (A) General diagram describing incorporation of a Lorentzian illumination intensity function into the radial cable model. (B) Calculation of developed fluorescence as a function of the integration shell. A finite number of points are sampled in each shell, as prescribed by the parameter n, the number of θ divisions. In the Center and Edge/Edge-tangent cases, illumination regions are proscribed by critical angles defined trigonometrically using the distance parameter, d. Those areas outside the critical angles are modeled as not contributing to fluorescence and carry an intensity value of zero.

where $RG = R_S \cdot \bar{G}_L \cdot a/2$.

Finally, for the innermost segment of the radial cable we have

$$2X \cdot u_{1,j+1} - (2X + 1) \cdot u_{0,j+1}$$

$$= -2X \cdot u_{1,j} + (\Delta T \cdot v^2 + 2X - 1) \cdot u_{0,j}$$

Incorporation of supercharging waveforms

Supercharging waveforms were formulated according to the following equations:

$$V_{COM}(t) = A_{step}(U(t) + A_1 e^{-(t/\tau_1)} + A_2 e^{-(t/\tau_2)} + A_3 e^{-(t/\tau_3)}),$$

$$0 < t \leq t_P$$

$$V_{COM}(t) = -A_{step}(A_1 e^{-((t-t_P)/\tau_1)} + A_2 e^{-((t-t_P)/\tau_2)}$$

$$+ A_3 e^{-((t-t_P)/\tau_3)}), \quad t > t_P$$

$V_{COM}(t)$ is the voltage-clamp command voltage, A_{step} is the amplitude of the step pulse in millivolts, $U(t)$ is the Heaviside step function, A_1-A_3 are the amplitudes of the three exponential functions in fractions of A_{step}, τ_1-τ_3 are the time constants of the three exponential functions in milliseconds, and t_P is the pulse length in milliseconds.

Voltage-clamp step pulses were simulated as an instantaneous jump in V_m. Supercharging waveforms were discretized at the same time interval used for numerical integration, which was 10 μs in all simulations.

APPENDIX B: ILLUMINATION ALGORITHMS

Within the framework of the distributed cable model with radial symmetry described in Appendix A, it was incumbent on us to derive a method whereby the varying illumination regions could be incorporated into the numerical integration process. The solution we developed allows the quantitative calculation of evoked fluorescence accounting for both regional illumination and the varying illumination intensity profile through a thick preparation.

Fig. 12 shows the intensity profile obtained with the 20× objective described in Materials and Methods. We found that a Lorentzian function provided a reasonable fit to the data and used the function with appropriate fit parameters (see Fig. 13 legend) as the predictive function for illumination intensity when calculating fluorescence in the radial cable model.

Fig. 13 outlines the general scheme employed for calculating developed fluorescence. The Lorentzian illumination profile was predefined as a continuous function as described above. This profile could be centered at any depth (as a function of the y axis in Fig. 13 A) in the cylindrical fiber. For each isopotential integration shell, s_i, a fluorescence geometry angle, θ, could be calculated. The fluorescence distance parameter, d, was assigned in any case in which the illumination paradigm was not Global.

During a simulation, the illumination algorithm was implemented after the voltage had been calculated for the entire cable at a given time point. It called for each integration shell to be broken up into a finite number of discrete sampling points, each defined by a voltage, an illumination intensity value, and an angle, θ_j. The voltage was calculated according to the procedure described in Appendix A, and the intensity was evaluated as a normalized function of y as defined in Fig. 13 A. The angle was obtained according to the number of divisions desired, as denoted in Fig. 13 B. At each sampling point, the developed fluorescence was calculated by multiplying the voltage by the intensity. The fluorescence of each shell was obtained by averaging the calculated fluorescence at each point. Homogeneous dye staining through the T-system was assumed.

The application of this algorithm to the Global, Center, and Edge/Edge-tangent illumination cases is depicted in Fig. 13 B. For the Global case, the entire fiber is illuminated, and each sampling point carries a nonzero intensity. In the Center and Edge/Edge-tangent cases, however, all points that fall in regions outside the illumination area carry a zero intensity and

thus do not contribute to the overall developed fluorescence. The fluorescence distance parameter, d, defines the Center and Edge/Edge-tangent illumination regions. For example, in the former case, $\cos^{-1}(d)$, $\pi - \cos^{-1}(d)$, $\pi + \cos^{-1}(d)$, and $-\cos^{-1}(d)$ are the four critical angles that determine the illumination boundaries. Similarly, for the latter case, $\cos^{-1}(d)$ and $-\cos^{-1}(d)$ define the boundaries. Any sampling point that falls outside these defined regions is set to zero intensity.

Clearly, a higher number of θ_j divisions affords a higher degree of accuracy, but also results in proportionally longer computation times. For the purposes of this work, no significant advantages were found by using >20 θ_j divisions, but significant error was encountered by using less than this number. As an alternative illumination algorithm, trapezoidal integration weighting of the circumference function, $2\pi r$, was also implemented. Because this approach is unable to account for illumination regions, it was used only as a comparison for global illumination results from the Lorentzian algorithm.

With respect to the experimental data and simulations presented in this work, varying the position of the peak of the illumination function within the confines of the mounted fiber had only minimal effects on the predicted fluorescence transients. This was to be expected, given the large depth of field and small range of intensities (relative to typical fiber dimensions) applicable with the 20× objective used. However, simulations with a more narrowly defined illumination function showed a proportionally greater influence of the illumination peak position parameter. The theoretical framework outlined here should be easily applicable to other thick preparation modeling scenarios in which illumination intensities are expected to vary.

REFERENCES

Adrian, R. H., W. K. Chandler, and A. L. Hodgkin. 1969a. The kinetics of mechanical activation in frog muscle. *J. Physiol. (Lond.).* 204:207–30.

Adrian, R. H., L. L. Costantin, and L. D. Peachey. 1969b. Radial spread of contraction in frog muscle fibres. *J. Physiol. (Lond.).* 204:231–257.

Adrian, R. H., and L. D. Peachey. 1973. Reconstruction of the action potential of frog sartorius muscle. *J. Physiol. (Lond.).* 235:103–131.

Armstrong, C. M., and R. H. Chow. 1987. Supercharging: a method for improving patch-clamp performance. *Biophys. J.* 52:133–136.

Ashcroft, F. M., J. A. Heiny, and J. Vergara. 1985. Inward rectification in the transverse tubular system of frog skeletal muscle studied with potentiometric dyes. *J. Physiol. (Lond.).* 359:269–291.

Bastian, J., and S. Nakajima. 1974. Action potential in the transverse tubules and its role in the activation of skeletal muscle. *J. Gen. Physiol.* 63:257–278.

Bedlack, R. S., Jr., M. Wei, and L. M. Loew. 1992. Localized membrane depolarizations and localized calcium influx during electric field-guided neurite growth. *Neuron.* 9:393–403.

Bezanilla, F., C. Caputo, H. Gonzalez-Serratos, and R. A. Venosa. 1972. Sodium dependence of the inward spread of activation in isolated twitch muscle fibres of the frog. *J. Physiol. (Lond.).* 223:507–523.

Blinks, J. R. 1965. Influence of osmotic strength on cross-section and volume of isolated single muscle fibres. *J. Physiol. (Lond.).* 177:42–57.

Crank, J. 1975. The Mathematics of Diffusion. Oxford University Press, Oxford.

Crank, J., and P. Nicolson. 1947. A practical method for numerical evaluation of solutions of partial differential equations of the heat conduction type. *Proc. Cambridge Philos. Soc.* 43:50–67.

Eisenberg, B. R. 1983. Quantitative ultrastructure of mammalian muscle. *In* Handbook of Physiology: Skeletal Muscle. L D. Peachey, R. H. Adrian, and S. R. Geiger, editors. American Physiological Society, Bethesda, MD. 355–379.

Falk, G. 1968. Predicted delays in the activation of the contractile system. *Biophys. J.* 8:608–625.

Falk, G., and P. Fatt. 1964. Linear electrical properties of striated muscle fibres observed with intracellular electrodes. *Proc. R. Soc. Lond. Ser. B.* 160:69–123.

Gerald, C. F. 1978. Applied Numerical Analysis. Addison-Wesley Publishing Company, Reading, MA.

Gonzalez-Serratos, H. 1971. Inward spread of activation in vertebrate muscle fibres. *J. Physiol. (Lond.).* 212:777–799.

Heiny, J. A., F. M. Ashcroft, and J. Vergara. 1983. T-system optical signals associated with inward rectification in skeletal muscle. *Nature.* 301: 164–166.

Heiny, J. A., and D. S. Jong. 1990. A nonlinear electrostatic potential change in the T-system of skeletal muscle detected under passive recording conditions using potentiometric dyes. *J. Gen. Physiol.* 95: 147–175.

Heiny, J. A., and J. Vergara. 1982. Optical signals from surface and T system membranes in skeletal muscle fibers. Experiments with the potentiometric dye NK2367. *J. Gen. Physiol.* 80:203–230.

Heiny, J. A., and J. Vergara. 1984. Dichroic behavior of the absorbance signals from dyes NK2367 and WW375 in skeletal muscle fibers. *J. Gen. Physiol.* 84:805–837.

Hille, B., and D. T. Campbell. 1976. An improved vaseline gap voltage clamp for skeletal muscle fibers. *J. Gen. Physiol.* 67:265–293.

Huxley, A. F., and R. E. Taylor. 1958. Local activation of striated muscle fibers. *J. Physiol.* 144:426–451.

Jong, D. S., K. Stroffekova, and J. A. Heiny. 1997. A surface potential change in the membranes of frog skeletal muscle is associated with excitation-contraction coupling. *J. Physiol. (Lond.).* 499:787–808.

Kim, A. M., and J. L. Vergara. 1998. Fast voltage gating of Ca^{2+} release in skeletal muscle revealed by supercharging pulses. *J. Physiol. (Lond.).* 511:509–518.

Nakajima, S., and A. Gilai. 1980. Action potentials of isolated single muscle fibers recorded by potential-sensitive dyes. *J. Gen. Physiol.* 76:729–750.

Palade, P., and J. Vergara. 1982. Arsenazo III and antipyrylazo III calcium transients in single skeletal muscle fibers. *J. Gen. Physiol.* 79:679–707.

Peachey, L. D. 1965a. The sarcoplasmic reticulum and transverse tubules of the frog's sartorius. *J. Cell Biol.* 25(Suppl.):209–231.

Peachey, L. D. 1965b. Transverse tubules in excitation-contraction coupling. *Fed. Proc.* 24:1124–1134.

Rohr, S., and B. M. Salzberg. 1994. Multiple site optical recording of transmembrane voltage. *Biophys. J.* 67:1301–1315.

Salzberg, B. M., and F. Bezanilla. 1983. An optical determination of the series resistance in Loligo. *J. Gen. Physiol.* 82:807–817.

Simon, B. J., and K. G. Beam. 1985. The influence of transverse tubular delays on the kinetics of charge movement in mammalian skeletal muscle. *J. Gen. Physiol.* 85:21–42.

Valdiosera, R., C. Clausen, and R. S. Eisenberg. 1974. Impedance of frog skeletal muscle fibers in various solutions. *J. Gen. Physiol.* 63:460–491.

Vergara, J. L., and F. Bezanilla. 1981. Optical Studies of E-C Coupling with Potentiometric Dyes. Academic Press, New York.

Vergara, J., F. Bezanilla, and B. M. Salzberg. 1978. Nile blue fluorescence signals from cut single muscle fibers under voltage or current clamp conditions. *J. Gen. Physiol.* 72:775–800.

Vergara, J., and M. Delay. 1986. A transmission delay and the effect of temperature at the triadic junction of skeletal muscle. *Proc. R. Soc. Lond. Biol.* 229:97–110.

Vergara, J., M. DiFranco, D. Compagnon, and B. A. Suarez-Isla. 1991. Imaging of calcium transients in skeletal muscle fibers. *Biophys. J.* 59:12–24.

Vergara, J. L., and A. M. Kim. 1997. Supercharging command pulses permit rapid voltage stepping of t-tubule membranes in skeletal muscle fibers. *Biophys. J.* 72:A274.

Zampighi, G., J. Vergara, and F. Ramon. 1975. On the connection between the transverse tubules and the plasma membrane in frog semitendinosus skeletal muscle. Are caveolae the mouths of the transverse tubule system? *J. Cell Biol.* 64:734–740.